Targeting mitochondrial double-stranded RNAs ameliorates autoimmune characteristics of Sjögren's syndrome

Authors: Jimin Yoon[1†], Min-Seok Lee[1†], Ahsan Ausaf Ali[1], Ye Rim Oh[2], Yong Seok Choi[2], Sujin Kim[1], Namseok Lee[1], Se Gwang Jang[3], Naseem Ahamad[4], Seung-Ki Kwok[5], Joon Young Hyon[6], Seunghee Cha[4], Yun Jong Lee[7,8*], Sung Gap Im[1,9*], Yoosik Kim[1,10*]

Affiliations:
[1]Department of Chemical and Biomolecular Engineering, Korea Advanced Institute of Science and Technology (KAIST), Daejeon 34141, Korea.
[2]Medical Science Research Institute, Seoul National University Bundang Hospital, Seongnam 13620, Korea.
[3]The Rheumatism Research Center, Catholic Research Institute of Medical Science, College of Medicine, The Catholic University of Korea, Seoul 06591, Korea.
[4] Department of Oral and Maxillofacial Diagnostic Sciences, University of Florida College of Dentistry, Gainesville, FL 32610, USA.
[5] Division of Rheumatology, Department of Internal Medicine, Seoul St. Mary's Hospital, College of Medicine, The Catholic University of Korea, Seoul 06591, Korea.
[6] Department of Ophthalmology, Seoul National University Bundang Hospital, Seongnam 13620, Korea.
[7]Division of Rheumatology, Department of Internal Medicine, Seoul National University Bundang Hospital, Seongnam 13620, Korea.
[8]Department of Internal Medicine, Department of Internal Medicine, Seoul National University College of Medicine, Seoul 03080, Korea.
[9]KI for NanoCentury (KINC), KAIST, Daejeon 34141, Korea.
[10]KI for Health Science and Technology (KIHST), KAIST, Daejeon 34141, Korea.

†: These authors contributed equally to this work as co-first authors.

*Correspondence should be addressed to Yoosik Kim: Tel: +82-42-350-7312; Fax: +82-42-350-3910; Email: ysyoosik@kaist.ac.kr. Correspondence may also be addressed to Yun Jong Lee: Tel: +82-31-787-7049; Fax: +82-31-787-4051; Email: yn35@snu.ac.kr and Sung Gap Im: Tel: +82-42-350-3976; Email: sgim@kaist.ac.kr.

Summary: Mitochondrial double-stranded RNA levels are elevated in the tear and saliva of SS patients. These RNAs promote type I interferon signature, as well as other autoimmune phenotypes in SS. Downregulation of mitochondrial dsRNAs alleviates autoimmune signatures of SS in salivary gland epithelial cells.

Abstract:

Sjögren's syndrome (SS) is a systemic autoimmune disease that targets the exocrine glands, resulting in impaired saliva and tear secretion. To date, type I interferons (IFNs) are increasingly recognized as pivotal mediators in SS, but their endogenous drivers have not been elucidated. Here, we investigate the role of mitochondrial double-stranded RNAs (mt-dsRNAs) in regulating type I IFN response in SS. We find that mt-dsRNAs are elevated in the saliva and tear of SS patients and in salivary glands of non-obese diabetic mice with salivary dysfunction. Using the in-house-developed 3D culture, we show that dsRNA stimulation increases mt-dsRNAs expression via JAK1/STAT pathway and facilitates their cytosolic export, which is accompanied by autoimmune signatures observed in SS. We further show that muscarinic receptor ligand acetylcholine or antioxidant resveratrol ameliorates autoimmune characteristics by preventing mt-dsRNA-mediated immune activation. In addition, direct suppression of mt-dsRNAs reverses the autoimmune signatures of SS. Altogether, our study underscores the significance of mt-dsRNA upregulation and suggests mt-dsRNAs as an important key to the puzzle of SS.

INTRODUCTION

Sjögren's syndrome (SS) is a slowly progressive autoimmune disorder characterized by lymphocytic infiltration of the exocrine glands, B cell hyperactivity with autoantibodies, and significant loss of secretory function, resulting in oral and eye dryness (Jin *et al*, 2013; Kroese *et al*, 2014; Qin *et al*, 2015). As with most autoimmune disorders, the etiology of SS is not yet fully understood. It is particularly challenging to establish the diagnosis due to individual patients with overlapping disease entities (Stefanski *et al*, 2017). Moreover, a therapeutic target of SS is unavailable as the treatment options depend on individual disease activity, and SS is diagnosed after the disease has progressed enough to cause significant pain. This delay is problematic because the patients' quality of life is significantly reduced by diverse manifestations of SS as well as numerous complications, including cardiovascular diseases and lymphoma (Stefanski *et al.*, 2017). Hence, it is important to expand our knowledge about the immunopathological mechanisms involved in SS to identify the targets for potential therapies and diagnosis.

One of the most notable features of SS is the type I interferon (IFN) signature (Crow *et al*, 2019). The type I IFNs can be produced in response to stimulation of pattern recognition receptors (PRRs) such as Toll-Like Receptors (TLRs), Protein Kinase R (PKR), and Melanoma Differentiation-Associated Gene 5 (MDA5) that recognize double-stranded RNAs (dsRNAs) (Huijser & Versnel, 2021; Kiripolsky & Kramer, 2018). Indeed, the upregulation of TLRs is often accompanied by increased levels of IFN-stimulated genes (ISGs) and proinflammatory cytokines, including Tumor Necrosis Factor-α (TNF-α), various interleukins (ILs), and IFN-γ in SS patients (Bikker *et al*, 2010). In particular, salivary glands with extensive mononuclear cell infiltration showed increased expression of type I IFNs and ISGs that are downstream targets of nucleic acid-sensing PRRs (Greenwell-Wild *et al*, 2011; Min *et al*, 2019). Consequently, the dysregulated

detection of nucleic acids has been established as one of the autoimmune signatures (Huijser & Versnel, 2021). Taken together, dsRNA-sensing PRRs may play an important role in engendering autoimmune phenotypes, and investigating both the identity and the roles of PRR-activating dsRNAs in the pathogenesis of SS is critical to understand type I IFN signature in SS.

Historically, long dsRNAs were associated with viral infection (Guo *et al*, 2019). However, recent evidence has shown that dsRNAs are also expressed endogenously and that they can initiate the immune response by activating PRRs (Ahmad *et al*, 2018; Kim *et al*, 2018). Among several types of endogenous dsRNAs, mt-dsRNAs are receiving increasing attention due to their strong biomedical implications in diseases such as alcohol-associated liver disease (Lee *et al*, 2020b), Huntington's disease (Lee *et al*, 2020a), and osteoarthritis (Kim *et al*, 2020). Mitochondria are able to generate dsRNAs due to bidirectional transcription of the mitochondrial genome. When present in the cytosol due to mutations in regulatory proteins or under stress, mt-dsRNAs are recognized by PRRs, such as PKR and MDA5, and initiate the downstream immune response (Dhir *et al*, 2018; Kim *et al.*, 2018). However, mt-dsRNA regulation and its pathophysiological role in SS still remain uninvestigated. Considering the excess level of oxidative stress and implications of mitochondrial dysfunction in chronic inflammation and tissue damages in SS (Cole *et al*, 2016; Hu *et al*, 2009; Pagano *et al*, 2013; Ryo *et al*, 2006), we hypothesized that mt-dsRNAs might participate in the activation of PRRs and drive the type I IFN response in SS.

In this study, we investigated the role of mt-dsRNAs in the pathogenesis of SS. We first analyzed the expression of both heavy and light strands of mitochondrial transcripts in saliva and tear samples of SS patients and analyzed the in vivo relevance using non-obese diabetic (NOD) mice with salivary dysfunction. We further investigated the role of mt-dsRNAs on SS-like autoimmune signatures, such as ISG induction, PKR activation, and altered expression of tight

junction complex (TJC) proteins and Aquaporin-5 (AQP5) water channel protein using salivary gland epithelial cells (SGECs) grown as three-dimensional (3D) spheroids. With the established 3D culture system, we examined whether muscarinic receptor (M3R) ligand acetylcholine (Ach) and antioxidant resveratrol (RES), two small molecules known to improve salivary function, suppressed SS-like autoimmune signatures via mt-dsRNA regulation. Lastly, we analyzed the effect of direct downregulation of mt-dsRNA expression on autoimmune signatures using an inhibitor of mitochondrial RNA polymerase (POLRMT). Together, our study uncovers the key regulatory function of mt-dsRNAs in exacerbating autoimmune characteristics in SS.

RESULTS

mt-dsRNA levels are elevated in saliva and tears of SS patients and salivary glands of aged NOD mice

We began our investigation by analyzing the expression levels of mt-dsRNAs because increased oxidative stress was reported in both mouse models and human samples of SS (Cole *et al.*, 2016; Hu *et al.*, 2009; Pagano *et al.*, 2013; Ryo *et al.*, 2006). We first measured mt-dsRNA levels in the saliva and tear samples collected from 73 and 16 study subjects, respectively. We extracted total RNAs from 200 μL of saliva and performed strand-specific reverse transcription to analyze the expression of heavy and light strand RNAs separately (Fig 1A). Among 16 RNAs analyzed, 15 of them showed higher median expression levels in all SS patients compared to non-SS sicca patients (Fig 1B). When compared to the non-sicca controls, 13 out of 16 RNAs showed higher expression levels in SS patients. Notably, all examined RNA expression patterns of the non-sicca control were indistinguishable from those of the non-SS sicca group. ANOVA analysis revealed statistically different (P-value < 0.05) expressions for 15 out of 16 RNAs. We also

examined mt-dsRNA expression patterns in 16 tear samples – 8 SS and 8 non-SS sicca subjects (Fig 1C). Similar to the saliva samples, higher levels of mt-dsRNAs were detected in SS. Most RNAs (14/15) tested showed higher expression in SS patients compared to the non-SS sicca controls. Collectively, our results suggest that mt-dsRNA expression patterns can be used to distinguish between non-SS sicca and SS patients.

We further analyzed our data and ranked the five most significant RNAs in tear and saliva samples respectively (Fig S1A and B). From both samples, *CYTB* heavy, *ND1* light, and *CO1* light strands were highly expressed in SS compared to non-SS sicca patients. When we analyzed the association between RNA levels in body fluid and exocrine dysfunction, we found that tear *CYTB* light strand levels were negatively correlated to tear production and positively correlated to the corneal and conjunctival damage (Fig S1C-E). Furthermore, salivary *ND5* heavy strand transcript levels showed a negative correlation to the stimulated whole salivary flow rates and a positive correlation to lymphocyte infiltration grade (Fig S1F-I).

Next, we investigated the expression of mt-dsRNAs in the epithelial cells of the salivary glands obtained from the NOD mice. Aged NOD mice develop SS-like autoimmune exocrinopathy, making them one of the most powerful tools in deciphering pathologic mechanisms of SS (Park *et al*, 2015). In our study, the salivary glands of NOD mice at different ages were analyzed. Since a significant decrease in the salivary flow rate of NOD mice after 17 weeks (Jonsson *et al*, 2006), we focused our analysis on NOD mice between 16 weeks and 28 weeks of age with 8 weeks mice as controls. We extracted total RNAs from 20 µm tissue sections of NOD mice salivary gland and measured the expression of five mt-dsRNAs – *Nd1*, *Nd5*, *Nd6*, *Co1*, and *Cytb* – which showed the most significant enrichment from the saliva samples of SS patients. Compared to that of 8-week-old NOD mice, expression levels for all mt-dsRNAs except *Cytb* were higher in NOD mice older

than 20 weeks (Fig 1D). Of note, due to high variance, ANOVA analysis did not yield any significant change despite a clear increase in the mean expression of the RNAs. Alternatively, we analyzed mt-dsRNA patterns by using single-molecule fluorescent RNA *in situ* hybridization (RNA-FISH). We clearly found that the expression of both *Nd5* heavy (*Nd5H*) and light strand (*Nd5L*) RNAs were elevated in acinar regions of NOD mice submandibular salivary gland tissues aged from 20 weeks to 28 weeks (Fig 1E), compared to the expression in 16-week mice. The increased expression of both heavy and light strand RNAs indicated the induction of mt-dsRNAs. Of note, the negative control probe yielded no signal (Fig 1F).

Antiviral signaling increases mt-dsRNA expression

Next, we investigated whether stimulating the antiviral signaling and type I IFN pathway in SGECs can elicit mt-dsRNA induction. In order to induce SS-like condition, we transfected SV-40 transformed salivary gland-squamous acinar cells (NS-SV-AC) with polyinosinic-polycytidylic acid (poly I:C), a synthetic analog of viral dsRNAs, for PRR stimulation. Repeated administration of poly I:C was reported to elicit IL-7 production and early inflammatory responses in the salivary gland and accelerate the development of SS-like sialadenitis (Deshmukh *et al*, 2009; Jin *et al.*, 2013). Moreover, poly I:C also led to other key characteristics of SS, such as leukocytic infiltration, antinuclear antibody production, and impaired tear secretion in mice (Zhou *et al*, 2015). We first analyzed the expression of ISGs associated with SS and the degree of PKR phosphorylation because the expression of PKR was increased in monocytes from IFN-positive SS patients (Maria *et al*, 2017) and various ISGs, such as MX1, IRF7, and IFI44 showed increased expression in the salivary tissues of the SS model (Kiripolsky & Kramer, 2018). Our data revealed strong ISGs

induction, increased PKR phosphorylation, and a consequential decrease in cell viability (Fig S2A-C).

We then measured the expression levels of mt-dsRNAs upon poly I:C stimulation. To our surprise, we found that the dsRNA stress to the salivary cells resulted in increased mt-dsRNA expression, both heavy and their complementary light strand RNAs (Fig S2D and E). Direct visualization of *ND5* mt-dsRNA via RNA-FISH further confirmed that both heavy and light strand RNAs showed increased expression (Fig S2F). We also analyzed the cytosolic presence of mt-dsRNAs to determine if mt-dsRNAs can interact with PRRs such as PKR to augment the antiviral signaling. We isolated RNAs from the free cytosolic compartment and analyzed the local mt-dsRNA expression via qRT-PCR. We found that poly I:C stimulated cells showed increased cytosolic mt-dsRNAs (Fig S2G). We also employed formaldehyde cross-linking and immunoprecipitation (fCLIP) to examine if released mt-dsRNAs interact with PKR. We found that PKR-mtRNA interaction was enhanced upon poly I:C stimulation (Fig S2H). Considering that both poly I:C and mt-dsRNAs can activate PKR, our results suggest that increased cellular mt-dsRNAs may amplify the effect of dsRNA-mediated antiviral signaling.

Additionally, we transfected poly I:C to primary SGECs as well as human parotid gland cells (HSY) to show that the observed elevation of mt-dsRNAs was not specific to NS-SV-AC. We found that SGECs obtained from SS patients exhibit higher mt-dsRNA expression levels compared to non-SS sicca patients (Fig S3A), although the sample number is too small to perform statistical analysis. Moreover, we analyzed mt-dsRNA expression upon transfection of dsRNAs and found that primary SGECs from both SS and non-SS sicca subjects (Fig S3B and C) and HSY cells (Fig S3D) all showed increased mt-dsRNA levels. Based on these results, we decided to use NS-SV-AC cells for the rest of our study.

dsRNA stress downregulates AQP5 and TJC proteins in 3D microenvironment

The aberrant activation of oral epithelial innate immune response is known to alter the expression and distribution of TJC proteins, which subsequently leads to destruction and secretory dysfunction of salivary and lacrimal glands (Groeger & Meyle, 2019), resulting in decreased quantity and quality of saliva (Ewert *et al*, 2010; Zhang *et al*, 2016). Moreover, the abnormal distribution of AQP5 protein is also evident in the salivary glands of SS patients (Lee *et al*, 2013; Steinfeld *et al*, 2001). However, there are limitations to studying the protein expression of TJC and AQP5 in 2D culture due to its weakness in replicating 3D microenvironment. Hence, in order to maintain cell-cell and cell-matrix interactions and reproduce physiological relevance in the context of 3D microenvironment, we employed a poly(2,4,6,7-tetravinyl-2,4,6,8-tetramethyl cyclotetrasiloxane) (pV4D4) functional polymer thin film platform to grow the acinar cells as 3D spheroids (Fig 2A). We chose the pV4D4-coated surface-based spheroid culture method because it can closely mimic in vivo microenvironment by inducing cell-extracellular matrix interactions with enhanced homogeneity in size distribution and circularity of NS-SV-AC compared to conventional options such as Ultra-Low attachment plate (ULA) (Fig S4A and B) (Choi *et al*, 2018; Yu *et al*, 2020). Indeed, we confirmed increased expression of TJC proteins (ZO-1 and Occludin) and AQP5 when cells were grown in 3D, and their expressions were too low in the conventional 2D culture system for robust analysis (Fig S4C and D).

With the established 3D culture system, we stimulated NS-SV-AC cells with poly I:C. Consistent with our results in 2D culture, ISGs and PKR phosphorylation were increased, and a decrease in cell viability was evident (Fig 2B-D). In addition, using the 3D system, we found that both ZO-1 and Occludin protein expressions were reduced significantly upon poly I:C stimulation

(Fig 2E). Moreover, the expression of laminin, a type of extracellular matrix (ECM) protein with reported degradation in SS (Schenke-Layland *et al*, 2008), also decreased upon poly I:C transfection in 3D culture (Fig S4E). Poly I:C stimulation also led to a dramatic decrease in AQP5 expression (Fig 2F and G). Of note, to analyze AQP5 expression, we used NS-SV-AC cells with stable expression of AQP5-GFP under the constitutive promoter. Last but not least, poly I:C transfection also led to the induction of mt-dsRNAs in our 3D culture system (Fig 2H).

mt-dsRNA induction occurs downstream of JAK1 pathway

Considering the close association between mt-dsRNA induction and autoimmune signatures of SS, such as TJC and AQP5 downregulation, ISGs induction, and PKR phosphorylation, we continued our investigation to identify the potential upstream pathway responsible for mt-dsRNA induction. We began our study by focusing on JAK-STAT pathway because both type I and II IFNs are known to activate JAK1, and a previous study reported that a selective JAK1 inhibitor is able to reduce IFN-inducible BAFF expression in SGECs (Lee *et al*, 2018; McInnes *et al*, 2019).

We first pretreated NS-SV-AC spheroids with upadacitinib, a JAK1 inhibitor, before poly I:C transfection. Our result showed that the pretreatment of upadacitinib significantly reduced the degree of ISGs induction (Fig 3A). Interestingly, the decreased ISGs induction was accompanied by reduced induction of mt-dsRNAs (Fig 3B). Therefore, our data suggest that the JAK1-STAT signaling pathway is responsible for the increased mt-dsRNA expression.

Effects of M3R ligand Ach are mediated via mt-dsRNAs

With our in-house developed 3D system, we investigated the relation between mtRNAs and the potential treatments for SS. Currently, patients are often prescribed a set of parasympathomimetic drugs that are known to mimic the effects of Ach. Parasympathomimetic drugs include pilocarpine and cevimeline, which bind to cholinergic (muscarinic) receptors and increase the secretion from the exocrine glands (Lopez-Lopez *et al*, 2014; Lopez-Pintor *et al*, 2015; Miranda-Rius *et al*, 2015). In addition, dysregulated salivation in SS is partly caused by the antagonistic immunoglobulins G (IgGs) against cholinergic receptors of exocrine glands, suppressing the glandular secretory function of M3R in SS (Cha *et al*, 2006; Passafaro *et al*, 2010).

First, we examined whether Ach could inhibit poly I:C-triggered ISGs and mt-dsRNA induction. We found that, in the presence of Ach, ISGs induction was significantly attenuated, and this phenomenon was accompanied by decreased induction of mt-dsRNAs (Fig 4A and B). To further validate the importance of mt-dsRNAs in mediating the effect of Ach on ISGs, we depleted mt-dsRNAs using 2- C′-methyladenosine (2-CM), an inhibitor of POLRMT. Pretreatment of 2-CM led to a dramatic decrease in the expression of all mt-dsRNAs examined (Fig 4C). We found that the effect of Ach was diminished in mt-dsRNA-depleted cells (Fig 4D), thereby suggesting that the suppression of ISGs by Ach was partly mediated by mt-dsRNAs.

We next analyzed whether the autoantibodies of SS patients could counteract the effect of Ach on suppressing ISG induction. We conducted a similar experiment as above, but this time, we also treated cells with either control human IgG or those pooled from four SS patients (denoted as SS-IgG). We found that SS-IgG resulted in increased ISGs induction and mt-dsRNA expression, thereby lessening the effect of Ach (Fig 4E and F). To further validate the adequacy of human IgGs used as the control, we compared the effect of control human IgG with IgG pooled from anti-

M3R negative rheumatoid arthritis (RA) patients (denoted as RA-IgG). The data showed indistinguishable differences in ISGs and mt-dsRNAs induction between control IgG and RA-IgG, thereby justifying the use of control human IgG as a negative control for SS-IgG (Fig 4G and H). Overall, our data indicate that SS-IgG may enhance the antiviral response via blockage of M3R interaction with Ach (Fig 4I). Moreover, this provides supporting evidence that the conventional parasympathomimetic drugs for SS may function by modulating cellular mt-dsRNA levels and localization.

Antioxidant RES improves SS-like features through mt-dsRNAs

In addition to M3R agonists, a previous study reported that administration of RES, a natural polyphenol with antioxidant and anti-inflammatory properties, resulted in increased saliva secretion in NOD mice (Inoue *et al*, 2016). We asked whether RES may also take part in alleviating dsRNA stress via modulating the levels of mt-dsRNAs. We pretreated NS-SV-AC spheroids with RES 24 h prior to poly I:C stimulation and examined the effect on downstream response. Through mRNA-seq, we confirmed that RES pretreatment significantly decreased the expression of genes related to the type I IFN signaling pathway (Fig 5A). Twenty-three out of 36 genes relevant to type I IFN showed decreased expression upon RES pretreatment, and we further validated sequencing results for a selected ISGs using qRT-PCR (Fig S5A). Gene ontology (GO) analysis clearly showed that genes related to antiviral immune response (both type I IFN and type II immune responses) were restored upon RES pretreatment (Fig S5B).

Upon RES pretreatment, cell viability was increased by 14.5 % (Fig 5B), and such protective effect may have been translated from reduced ISGs induction and reduced PKR activation (Fig 5C). We then examined the expression of ZO-1, Occludin, and AQP5 and found

that the expression levels of the aforementioned proteins were all restored to nearly normal (Fig 5D-F). Most interestingly, when we examined the expression of mt-dsRNAs, we found that RES pretreatment decreased the mt-dsRNA levels in poly I:C stimulated cells (Fig 5G). This suggests that the antioxidant RES relieves dsRNA-mediated antiviral signaling partly by protecting mitochondria and preventing the induction and subsequent cytosolic release of mt-dsRNAs.

Targeting mt-dsRNAs ameliorates the autoimmune signatures of SS

In order to test the accountability of mt-dsRNAs in amplifying antiviral signaling and exacerbating autoimmune characteristics of SS, we analyzed the effect of poly I:C stimulation in mtRNA-depleted cells. Through mRNA-seq, we found that 2-CM pretreatment significantly decreased the expression of genes related to the type I IFN signaling pathway (Fig 6A). Half the number of genes relevant to type I IFN signaling showed reduced levels upon 2-CM pretreatment, and such a result was further confirmed using qRT-PCR (Fig S6A). While poly I:C transfection still induced ISGs, the degree of induction was significantly reduced when mt-dsRNAs were downregulated, suggesting that the increased expression of mt-dsRNAs and their cytosolic export in wild-type cells may aggravate the immune response triggered by poly I:C stimulation. The GO analysis revealed that genes related to oxidative phosphorylation (4.55%) and negative regulation of viral genome replication (18.18%) were partly rescued upon 2-CM pretreatment (Fig S6B). Moreover, similar to RES pretreatment, 2-CM resulted in decreased induction of genes involved in lymphocyte chemotaxis (3.03%). Of note, the results of RES pretreatment were strikingly similar to those of 2-CM, further supporting that the effect of RES might be mediated by mt-dsRNAs.

Downregulation of mt-dsRNAs also rescued cell proliferation by approximately 10% (Fig 6B), and again, this was potentially due to decreased ISGs and reduced phosphorylation of PKR (Fig 6C). We examined the effect of 2-CM pretreatment in the expression of TJCs and AQP5 proteins. 2-CM pretreatment counteracted the effect of poly I:C and almost completely rescued the expression of ZO-1 and Occludin (Fig 6D) as well as AQP5 (Fig 6E and F). Altogether, these results indicate that direct suppression of mt-dsRNAs can rescue autoimmune features of SS.

DISCUSSION

We here report the important roles of mt-dsRNAs in enhancing autoimmune features of SS. Our data clearly demonstrated that 1) mt-dsRNAs were characteristically elevated in SS patients and that their levels were negatively associated with exocrine dysfunction and sialadenitis; 2) mt-dsRNAs were increased in salivary glands of SS mouse model; 3) activation of dsRNA-mediated antiviral signaling led to increased mt-dsRNA expression in SGECs; 4) mt-dsRNA induction was under the control of the JAK1-STAT signaling pathway; 5) the protective effect of M3R ligand Ach was mediated partly by mt-dsRNAs, and SS-IgG negated such protective action of Ach; 6) antioxidant treatment decreased mt-dsRNA expression and autoimmune features of SS; 7) finally, direct downregulation of mt-dsRNAs ameliorated the autoimmune phenotypes of SS (Fig 7).

Our study provides a potential link between mitochondrial damage and the activation of PRRs, which subsequently leads to upregulation of type I IFN. Based on the evidence that mitochondrial dysfunction and accumulation of damaged mitochondria are frequently reported in SS patients (Barrera *et al*, 2021; Rai *et al*, 2021), we began our study by stimulating SGECs with poly I:C to yield reactive oxygen species (ROS) stress and disruption of mitochondrial potential (Chen *et al*, 2016; Harashima *et al*, 2014). We found that poly I:C stimulation resulted in the

cytosolic release of mt-dsRNAs, and subsequent PKR phosphorylation and ISG induction. Notably, mt-dsRNA induction and their cytosolic release were essential to augment the antiviral response. Indeed, downregulation of mt-dsRNAs via 2-CM resulted in the attenuation of IFN signature. Considering that mt-dsRNAs can be exported outside the cells and work as extracellular signaling molecules (Kim *et al.*, 2020; Lee *et al.*, 2020b), mt-dsRNAs may play a pathogenic mediator of IFN-derived inflammation in the exocrine glands of SS. Indeed, through various routes, mitochondria are actively involved in the activation of PRRs and innate immune responses, leading to type I IFN and inflammatory responses (Riley & Tait, 2020).

Our data also indicate that there exists nuclear-mitochondrial communication when cells are under dsRNA stress, leading to the mt-dsRNA accumulation and release. However, genes involved in this process and their molecular mechanism are yet to be determined. Our RNA-seq data provide a potential direction in identifying such factors. Closer examination of DEGs revealed that genes involved in mt-dsRNA stability, such as SLIRP, showed increased expression in poly I:C stimulated cells. Consistent with our hypothesis, SLIRP has been shown to protect the mitochondrial RNAs from degradation (Lagouge *et al*, 2015), and this may explain how mt-dsRNAs were protected from degradation and resulted in rapid accumulation upon poly I:C stimulation. Additionally, the expression of BCL-2 interacting protein 3 (BNIP3), which is responsible for the regulation of mitophagy (Zhang & Ney, 2009), was increased. Considering that other BCL-2 family proteins – BAX and BAK – are involved in the mitochondrial outer-membrane permeabilization (MOMP) (Pena-Blanco & Garcia-Saez, 2018), BNIP3 may also play a role in the cytosolic release of mt-dsRNAs through MOMP. Overall, the current study suggests dsRNA stress increases the expression of transcripts that can alter mitochondrial homeostasis and gene induction,

thereby providing valuable evidence to further investigate the therapeutic potential of targeting mt-dsRNA transcription or cytosolic transport in SS.

Although there is no cure for SS, known medications that are prescribed to alleviate the pains of SS patients are partly dependent on mt-dsRNA modulation. Firstly, we showed that there are clear links between the action mechanism of SS-IgG and mt-dsRNAs. Autoantibodies from SS patients, including anti-M3R autoantibodies, reportedly inhibited the secretory function of exocrine tissues in NOD mice (Robinson *et al*, 1998) and suppressed cholinergic-induced Ca^{2+} mobilization and AQP5 trafficking in SGECs (Li *et al*, 2004). Hence, the long-term administration of approved muscarinic agonist drugs such as pilocarpine was reported to increase M3R expression in the salivary gland (Minagi *et al*, 2018). Yet, the potential target molecule to diminish such an action mechanism has not been identified. Here, we fill this gap by showing that Ach reduces ISG levels in SGECs by preventing mt-dsRNA induction. The interrelationship of mt-dsRNAs with M3R and SS-IgG can be further investigated to elucidate how the aberrant autoimmune response leads to sicca symptoms. In addition, we also investigated the effect of antioxidant RES, which is known to improve salivary flow in NOD mice. Our data successfully demonstrated that RES ameliorates the degree of mt-dsRNAs induction, thereby yielding protective effects against SS-like autoimmune phenotypes in SGECs. Lastly, we tested the effect of upadacitinib, a JAK1 inhibitor approved for RA treatment, to suggest a potential upstream signaling pathway responsible for mt-dsRNA induction. Our results provide another scientific evidence to support a clinical trial of JAK1 inhibitor in SS. Indeed, due to the ability of JAK inhibitors to suppress ROS- or IFN-induced activation of SGECs, a phase 2 clinical trial is ongoing to assess the safety and efficacy of fligotinib, another JAK1 inhibitor, in SS patients (You *et al*, 2020).

There still lies limitations in our study in that we were unable to identify the cellular origin of salivary and tear dsRNAs. As mt-dsRNAs are significantly elevated in the saliva and tear samples of SS patients compared to healthy or non-SS sicca subjects, mt-dsRNAs can be used as a pathophysiological biomarker for earlier diagnosis of SS. Yet, the cellular origin and the mechanism behind how these dsRNAs arrive in saliva or tear still remain unanswered. The majority of mt-dsRNAs may be released from stressed epithelial cells in the oral mucosa or kerato-conjunctiva. Still, it will be helpful to find the sources of salivary and tear mt-dsRNAs, since it will provide further hints in developing targeted treatment options for SS.

In sum, our study highlights the importance of mt-dsRNA induction and their cytosolic release in enhancing dsRNA-mediated immune responses and potentiating autoimmune phenotypes in SGECs. This knowledge will have potential implications for the design of targeted therapies to remove accumulated mt-dsRNAs or encourage mt-dsRNA decay to ultimately ameliorate autoimmune characteristics of SS and successfully combat the disease.

MATERIALS AND METHODS

Patient saliva and tear samples

From 42 patients with SS, 31 patients with non-SS sicca, and 16 non-sicca voluntary donors, saliva (34 SS, 23 non-SS sicca, and 16 non-sicca controls) or tears (8 SS and 8 non-SS sicca samples) were collected. SS was classified according to the 2016 American College of Rheumatology/European League Against Rheumatism (ACR/EULAR) classification criteria for primary SS (Shiboski *et al*, 2017) and non-SS sicca subjects did not fulfill the ACR/EULAR criteria and the 2002 revised American-European Consensus Group criteria (Vitali *et al*, 2002). Their clinical characteristics are summarized in Table S1.

After application with 50 µl of normal saline in the inferior fornix and blinking for 5 sec, tear samples were collected from the inferior tear meniscus using glass capillary tubes (Corning). Schirmer test and ocular surface staining scoring were performed to assess tear production and the severity of keratoconjunctivitis sicca, respectively (Whitcher *et al*, 2010). Saliva samples were collected as described previously (Lee *et al*, 2010). Unstimulated and stimulated whole salivary flow rates were measured at the time of saliva sample collection. Tear and saliva samples were stored at -70℃ until further analysis. All participants provided written informed consent and sample collection was approved by the Institutional Review Board (B-0506/021-004 and B-1806-472-301) of Seoul National University Bundang Hospital.

NOD mice SG tissue histology

All procedures of animal research were provided in accordance with the Laboratory Animals Welfare Act, the Guide for the Care and Use of Laboratory Animals and the Guidelines and Policies for Rodent experiment provided by the IACUC (Institutional Animal Care and Use Committee) in school of medicine, The Catholic University of Korea (Approval numbers: CUMS-2019-0255-01). Female NOD/ShiLtJ mice were purchased from The Jackson Laboratory. The animals were maintained under specific pathogen-free conditions from age 8 weeks to age 28 weeks. Mouse submandibular SG tissues were fixed in formalin and embedded in paraffin.

Cell culture and chemical treatment

SV40-immortalized NS-SV-AC cell was provided by Professor Masayuki Azuma (Department of Oral Medicine, University of Tokushima Graduate Faculty of Dentistry, Japan) (Azuma *et al*, 1993). NS-SV-AC human salivary gland acinar cells were grown in Keratinocyte-SFM (Serum free media; Gibco) supplemented with 10% (v/v) heat-inactivated fetal bovine serum (FBS; Welgene) and 1% (v/v) 100x penicillin-streptomycin (Gibco). pGFP-hAQP5-C1 plasmid from Professor Kyung Pyo Park (Seoul National University, South Korea), was used to develop hAQP5-expressing NS-SV-AC cell line under the constitutive promoter (100 µg/ml of G418 selection). All cells were maintained at 37℃ in a humidified 5% CO_2 incubator. HSY cells were grown in Dulbecco's modified eagle medium (DMEM; Welgene) supplemented with 10 % (v/v) fetal bovine serum (FBS; Gibco).

To induce dsRNA stress, 20 µg/ml of poly I:C (Sigma Aldrich) was transfected using Lipofectamine 3000 (Thermo Fisher Scientific) for 14 h following the manufacturer's guide. As for the controlled mock transfection, RNase-free water (Diethyl pyrocarbonate (DEPC)-treated water) was used.

To test the effect of Ach or SS-IgG on mt-dsRNAs induction, 100 µM of Ach (Sigma Aldrich) was co-treated with poly I:C transfection. Human IgG was prepared from 4 SS patients with anti-M3 muscarinic acetylcholine receptor antibodies (Mona *et al*, 2020), using the NAb^{TM} Spin Kits for antibody purification (Thermo Fisher Scientific). IgG was pooled from four individual SS patients (125 µg/patient) and then mixed to the total mass of 500 µg, then lyophilized. The same method was used to pool IgG from four individual RA patients (125 µg/patient). IgG from human serum (Sigma Aldrich) was used as a control. All IgGs were dissolved in 150 mM NaCl before treatment. To test the effect of antioxidant on mt-dsRNA, 20 µM of RES (Sigma Aldrich) was pretreated for 24 h prior to poly I:C transfection. To examine the therapeutic effect of JAK1 inhibitor, 1 µg/mL of upadacitinib (MedKoo Biosciences) was treated 1 h prior to poly I:C transfection. To downregulate mt-dsRNAs expression, 20 µM of 2-CM (Santa Cruz Biotechnology) was pretreated 24 h prior to poly I:C transfection.

Primary SGEC culture of SS patients

Patients were diagnosed as having primary SS according to the American-European Consensus Group criteria (Vitali *et al.*, 2002). Informed consent was obtained from all patients according to the principles of the Declaration of Helsinki. Labial salivary gland biopsy tissues were obtained from control patients with sicca symptoms as well as from patients with primary SS. This study was approved by the Institutional Review Board of Seoul St. Mary's Hospital (approval no. KC13ONMI0646). Lip biopsy samples were minced in 1 unit/ml of Dispase solution (StemCell Technologies) containing 2 mg/ml of collagenase IV (Gibco) and were then digested with gentle resuspension. Primary salivary gland epithelial cells (SGECs) were cultured in Dulbecco's modified Eagle's Medium-Ham's F-12 (1:3) (Gibco) containing 2.5% fetal bovine serum (Gibco), 1% penicillin-streptomycin (Gibco), 0.4 μg/ml hydrocortisone (Sigma), 10 ng/ml epidermal growth factor (EGF; BioLegend), and 0.5 μg/ml insulin (Gibco). Single-cell suspensions were transferred to bovine type I collagen (PureCol; Advanced BioMatrix)-coated culture dishes.

RNA extraction and quantitative real-time PCR

To extract total RNAs from cultured cell, TRIzol (Ambion) was added directly to the cell pellet obtained after centrifugation at 10,000 *x g* for 30 sec. After precipitation of the extracted nucleic acids, DNase I (TaKaRa) was treated to remove DNA, and purified RNA was reverse transcribed using RevertAid reverse transcriptase (Thermo Fisher Scientific). For RNA extracted from patient samples and 3D spheroids, SuperScript IV Reverse Transcriptase (Invitrogen) was used to synthesize cDNA. For strand-specific qRT-PCR, reverse transcription primers containing CMV promoter sequences were designed to target the specific genes. cDNA was amplified by SYBR Green PCR master mix (Bioline) and qRT-PCR was performed using AriaMx Real-time PCR system (Agilent) and QuantStudio 1 Real-time PCR system (Thermo Fisher Scientific). Primers used in the study are provided in Table S2-S4. To analyze the localization of mtRNAs, cytosolic RNAs were isolated from cell lysates using the subcellular protein fractionation kit (Thermo Fisher Scientific) following the manufacturer's instruction. TRIzol LS (Ambion) was added individually at a 3:1 ratio to the cytosolic fraction to extract the RNAs. The rest of the steps were the same as above.

To extract RNA from NOD mice SG tissue, 20 µm-sections were dewaxed using xylene, then dehydrated in ethanol according to a previously published protocol (Ma, 2012). Same reagents were used to synthesize cDNA and mice-specific primers were used for qRT-PCR analysis.

Western Blotting

Cell lysates were prepared by incubating cells in the lysis buffer (50 mM Tris-HCl pH 8.0, 100 mM KCl, 0.5% NP-40, 10% Glycerol, and 1 mM DTT) supplemented with a protease inhibitor cocktail (Merck) followed by sonication. 30 - 40 µg of protein samples were loaded and separated on a 10% SDS-PAGE gel, and transferred to a PVDF membrane (Merck) using an Amersham semi-dry transfer system. The primary antibodies used in this study were as follows: GFP (Sigma Aldrich; G1544), GAPDH (Santa Cruz Biotechnology; 6C5 sc-32233), pPKR (Abcam, Ab81303), PKR (Cell Signaling Technology, D7F7), and β-tubulin (Cell Signaling Technology).

Acid phosphatase assay (APH)

Cells (or spheroids) were centrifuged for 10 min at 400 *x g* for spin down. After washing the pellets twice with DPBS (Welgene, LB001-02), the supernatant was discarded to obtain the final volume of 100 µl. 100 µl of APH assay buffer (0.1 M sodium acetate, 0.1% (v/v) Triton X-100 (Promega), 2 mg/ml Immunopure PNPP (Sigma Aldrich) in deionized/distilled water) was added to each well and incubated for 90 min at 37℃ with 5% CO_2. After incubation, 10 µl of 1N NaOH was added, and absorption at 405 nm was measured on a microplate reader (BioTek). For each experiment, cell viability was normalized to the data from the control group without poly I:C transfection.

Immunocytochemistry and RNA single-molecule fluorescent *in situ* hybridization

Spheroids from pV4D4-coated plates were transferred to a 1.5 ml tube, and analysis for 2D culture was performed on a confocal dish (SPL). Cells were fixed in 4% (w/v) paraformaldehyde for 15 min at room temperature. Fixed cells were then permeabilized with 0.3% (w/v) Triton X-100 (Sigma Aldrich) in Dulbecco's phosphate-buffered saline (DPBS) for 10 min at room temperature and blocked in 3% bovine serum albumin (BSA100; Bovogen) for 1 h. Cells were incubated with primary antibodies diluted in 1% BSA at a 1:100 ratio overnight at 4℃. The primary antibodies used in this study include: Occludin (Invitrogen; OC-3F10) and ZO-1 (Cell Signaling Technology; 8193S). Cells were then washed with DPBS and incubated with Alexa fluor 488-conjugated anti-

mouse secondary antibody (Thermo Fisher Scientific; A31570) and Alexa fluor 555 conjugated anti-mouse secondary antibody (Thermo Fisher Scientific; A-21202) diluted at a 1:1000 ratio for 45 min at room temperature. DAPI was incubated for 5 min. All washing steps for spheroids include centrifugation (5 min, 200 g) and supernatant discarding. Fluorescent images were obtained using a confocal laser-scanning microscope (LSM 880, Carl Zeiss). The fluorescence intensity per area was quantified as integrated density divided by the area of each spheroid and then normalized to the control without poly I:C transfection.

To visualize heavy and light strands of mt-Nd5 mtRNA from NOD mice SG tissue, five-micrometer sections were dewaxed using xylene, then dehydrated in ethanol for staining with RNAscope RNA fluorescent *in situ* hybridization (ACD) probes. The pretreatment, hybridization, and signal amplification were done following the manufacturer's instructions. Zeiss LSM 780 confocal microscope using 63x (NA = 1.40) objectives was used for visualization.

PKR fCLIP

To prepare PKR antibody-conjugated beads, protein A beads (Thermo Fisher Scientific) were incubated with PKR antibody (Cell Signaling Technology) in the fCLIP lysis buffer (20 mM Tris-HCl, pH 7.5, 15 mM NaCl, 10 mM EDTA, 0.5% NP-40, 0.1% Triton X-100, 0.1% SDS, and 0.1% sodium deoxycholate) for 3 h at 4°C after adjusting NaCl concentration to 150 mM. Harvested cells were fixed with 0.1% (w/v) paraformaldehyde (Sigma Aldrich) for 10 min and immediately quenched by adjusting glycine (Bio-basic) concentration to 250 mM for an additional 10 min at room temperature. The cross-linked cells were lysed using the fCLIP lysis buffer for 10 min on ice and then sonicated. The NaCl concentration of the lysate was adjusted to 150 mM, and cell debris was separated by centrifugation. The lysate was added to the PKR antibody-conjugated beads and incubated for 3 h at 4°C. The beads were washed 4 times with the fCLIP wash buffer (20 mM Tris-HCl, pH 7.5, 150 mM NaCl, 10 mM EDTA, 0.1% NP-40, 0.1% SDS, 0.1% Triton X-100, and 0.1% sodium deoxycholate) and PKR-dsRNA complex was eluted from the beads by incubating in the elution buffer (200 mM Tris-HCl, pH 7.4, 100 mM NaCl, 20 mM EDTA, 2% SDS, and 7 M Urea) for 3 h at 25°C. The eluate was treated with 2 mg/ml proteinase K (Sigma Aldrich) for overnight at 65°C. RNA was purified using acid-phenol:Chloroform pH 4.5 (Thermo Fisher Scientific).

Polymer thin films via the initiated chemical vapor deposition process

A 300 nm-thick pV4D4 film was deposited directly onto tissue culture polystyrene (TCPS) via the initiated chemical vapor deposition (iCVD) process. TCPS was first placed on the stage of a custom-built iCVD chamber. V4D4 (97%; Jihyunchem Co.) was heated to 70°C for monomer vaporization. The vaporized monomer V4D4, and the initiator, *tert*-butyl peroxide (TBPO; 95%; Sigma Aldrich) were introduced into the iCVD chamber at flow rates of 1.94 and 0.744 sccm, respectively. The pressure of the chamber was set to 260 mTorr. To decompose TBPO to generate radicals, the filament temperature was heated to 200℃. During the deposition process, the stage was maintained to 38.5℃ for the adsorption of monomers.

3D spheroid culture on a pV4D4-coated plate

Cells were seeded at the density of $1x10^5$ cells/ml on a pV4D4-coated plate and cultured in the same media described above and maintained at 37℃ in a humidified 5% CO_2 incubator. The spheroids formed on the pV4D4-coated plate were imaged at 24, 48, and 72 h after seeding by phase-contrast microscopy (Eclipse Ti-U; Nikon). For the live-imaging of spheroid formation, cells were monitored using an optical microscope (LumaScope 620 System; Etaluma). Images were acquired every 2 min for 24 h with a 10X magnification.

Data analysis of mRNA-seq data

Read files were quality checked with FastQC. Reads were aligned to the human genome (hg38) using Hisat2 (ver 2.1.0) (Kim *et al*, 2019). The aligned reads were quantified with StringTie (Pertea *et al*, 2015) using human gene annotation file version 32 from Gencode as the index. Differentially expressed genes were searched with DESeq2 (Love *et al*, 2014).

Differentially expressed gene (DEG) analysis

For DEG analysis, DESeq2 analysis (Love *et al.*, 2014) was performed three times separately in each of DMSO, 2-CM, and RES-pretreated groups. Within each group, raw counts of two biological replicates with poly I:C transfection were compared against the raw counts of two replicates with the control group (i.e. DEPC transfection). The counts were normalized by DESeq2

during analysis. The analysis yielded three separate lists of differentially expressed genes, and the genes were ordered by the lowest adjusted p-values for further analysis.

Gene ontology (GO) analysis of differentially expressed RNAs

Among genes that show log2 fold change with p-values less than 0.05, the values of DMSO (i.e. control) were subtracted from those of RES or 2-CM-pretreated RNAs to evaluate the degree of rescue in the induction of gene expression. Top 200 of the genes that show rescue effects were assembled into a gene list for GO analysis. GO analysis was done using the ClueGo software (Cytoscape, v. 3.7.1) (Bindea *et al*, 2009).

Statistical Analysis

Quantitative RT-PCR data and APH assay results were analyzed using the one-tailed Student's t-test. All data were biologically replicated at least three times. The error bars indicate the standard error of the mean. p-values ≤ 0.05 were regarded as statistically significant. * denotes p-values ≤ 0.05, ** is p-values ≤ 0.01, and *** is p-values ≤ 0.001.

Online supplemental material: Online supplemental material is available.

Data and materials availability: All data needed to evaluate the conclusions in the paper are present in the paper and/or the Supplementary Materials. Additional data related to this paper may be requested from the first and/or corresponding author/s. Sequencing data that support the findings of this study are available in the GEO database under the accession number GSE168148. All other relevant datasets used and/or analyzed during the current study are available within the article and its Supplementary Materials files or from the corresponding authors on reasonable request. The computational pipeline used in this study is open-sourced and available at: https://daehwankimlab.github.io/hisat2/ , https://ccb.jhu.edu/software/stringtie/ , and http://www.bioconductor.org/packages/release/bioc/html/DESeq2.html.

Acknowledgments: We thank all members of the Lee, Im, and Kim laboratory for helpful discussion and comments on the paper.

Funding: This work was supported by the Ministry of Health & Welfare (HI21C1501, to Y.K.), KAIST-SNUBH End-Run Project (N11180151, to Y.K. and No. 16-2018-003 to Y.J.L.), Technology Innovation Program (No. 20008777, to S. I.) by the Ministry of Trade, Industry and Energy (MOTIE, Korea), and the Sjögren's Foundation and NIH/NIAIMS (AR079693, to S.C.).

Author contributions: J. Yoon, M. Lee, YJ. Lee, SG. Lim, and Y. Kim designed the study and analysis. Experiments were performed by J. Yoon, and M. Lee performed imaging and cell viability analysis of 3D spheroids. YJ. Lee provided the saliva samples. A.A. Ali analyzed the saliva samples and performed the initial characterization of 3D spheroids. YR. Oh and YS. Choi collected and prepared patient samples and developed an hAQP5-expressing NS-SV-AC cell line. N. Lee processed the mRNA-seq raw data file for DEG analysis. SG. Jang and S. Kwok provided the NOD mouse tissue samples and primary cells of SS patients. J. Yoon and S. Kim analyzed the salivary gland tissues of NOD mice. JY. Hyon and S. Cha designed the project with YJ. Lee. The study was supervised by Y. Kim, YJ. Lee, and SG. Im. J. Yoon and Y. Kim wrote the manuscript with contributions from N. Ahamad, S. Cha, and S. Kim. All authors subsequently reviewed and edited the manuscript.

Competing interests: S.G.I. is a co-inventor of the polymeric thin film-based 3D culture used in this study and is currently filing a patent for it. The authors declare no competing interests.

References

Ahmad S, Mu X, Yang F, Greenwald E, Park JW, Jacob E, Zhang CZ, Hur S (2018) Breaching Self-Tolerance to Alu Duplex RNA Underlies MDA5-Mediated Inflammation. *Cell* 172: 797-810 e713

Azuma M, Tamatani T, Kasai Y, Sato M (1993) Immortalization of normal human salivary gland cells with duct-, myoepithelial-, acinar-, or squamous phenotype by transfection with SV40 ori-mutant deoxyribonucleic acid. *Lab Invest* 69: 24-42

Barrera MJ, Aguilera S, Castro I, Carvajal P, Jara D, Molina C, Gonzalez S, Gonzalez MJ (2021) Dysfunctional mitochondria as critical players in the inflammation of autoimmune diseases: Potential role in Sjo & uml;gren's syndrome. *Autoimmunity Reviews* 20

Bikker A, van Woerkom JM, Kruize AA, Wenting-van Wijk M, de Jager W, Bijlsma JW, Lafeber FP, van Roon JA (2010) Increased expression of interleukin-7 in labial salivary glands of patients with primary Sjogren's syndrome correlates with increased inflammation. *Arthritis Rheum* 62: 969-977

Bindea G, Mlecnik B, Hackl H, Charoentong P, Tosolini M, Kirilovsky A, Fridman WH, Pages F, Trajanoski Z, Galon J (2009) ClueGO: a Cytoscape plug-in to decipher functionally grouped gene ontology and pathway annotation networks. *Bioinformatics* 25: 1091-1093

Cha S, Singson E, Cornelius J, Yagna JP, Knot HJ, Peck AB (2006) Muscarinic acetylcholine type-3 receptor desensitization due to chronic exposure to Sjogren's syndrome-associated autoantibodies. *J Rheumatol* 33: 296-306

Chen H, Wang DL, Liu YL (2016) Poly (I:C) transfection induces mitochondrial-mediated apoptosis in cervical cancer. *Mol Med Rep* 13: 2689-2695

Choi M, Yu SJ, Choi Y, Lee HR, Lee E, Lee E, Lee Y, Song J, Son JG, Lee TG *et al* (2018) Polymer Thin Film-Induced Tumor Spheroids Acquire Cancer Stem Cell-like Properties. *Cancer Res* 78: 6890-6902

Cole MB, Quach H, Quach D, Baker A, Taylor KE, Barcellos LF, Criswell LA (2016) Epigenetic Signatures of Salivary Gland Inflammation in Sjogren's Syndrome. *Arthritis Rheumatol* 68: 2936-2944

Crow MK, Olferiev M, Kirou KA (2019) Type I Interferons in Autoimmune Disease. *Annu Rev Pathol* 14: 369-393

Deshmukh US, Nandula SR, Thimmalapura PR, Scindia YM, Bagavant H (2009) Activation of innate immune responses through Toll-like receptor 3 causes a rapid loss of salivary gland function. *J Oral Pathol Med* 38: 42-47

Dhir A, Dhir S, Borowski LS, Jimenez L, Teitell M, Rotig A, Crow YJ, Rice GI, Duffy D, Tamby C *et al* (2018) Mitochondrial double-stranded RNA triggers antiviral signalling in humans. *Nature* 560: 238-242

Ewert P, Aguilera S, Alliende C, Kwon YJ, Albornoz A, Molina C, Urzua U, Quest AF, Olea N, Perez P *et al* (2010) Disruption of tight junction structure in salivary glands from Sjogren's syndrome patients is linked to proinflammatory cytokine exposure. *Arthritis Rheum* 62: 1280-1289

Greenwell-Wild T, Moutsopoulos NM, Gliozzi M, Kapsogeorgou E, Rangel Z, Munson PJ, Moutsopoulos HM, Wahl SM (2011) Chitinases in the salivary glands and circulation of patients with Sjogren's syndrome: macrophage harbingers of disease severity. *Arthritis Rheum* 63: 3103-3115

Groeger S, Meyle J (2019) Oral Mucosal Epithelial Cells. *Front Immunol* 10: 208

Guo Z, Li Y, Ding SW (2019) Small RNA-based antimicrobial immunity. *Nat Rev Immunol* 19: 31-44
Harashima N, Minami T, Uemura H, Harada M (2014) Transfection of poly(I:C) can induce reactive oxygen species-triggered apoptosis and interferon-β-mediated growth arrest in human renal cell carcinoma cells via innate adjuvant receptors and the 2-5A system. *Molecular cancer* 13: 217-217
Hu S, Zhou M, Jiang J, Wang J, Elashoff D, Gorr S, Michie SA, Spijkervet FK, Bootsma H, Kallenberg CG *et al* (2009) Systems biology analysis of Sjogren's syndrome and mucosa-associated lymphoid tissue lymphoma in parotid glands. *Arthritis Rheum* 60: 81-92
Huijser E, Versnel MA (2021) Making Sense of Intracellular Nucleic Acid Sensing in Type I Interferon Activation in Sjogren's Syndrome. *J Clin Med* 10
Inoue H, Kishimoto A, Ushikoshi-Nakayama R, Hasaka A, Takahashi A, Ryo K, Muramatsu T, Ide F, Mishima K, Saito I (2016) Resveratrol improves salivary dysfunction in a non-obese diabetic (NOD) mouse model of Sjogren's syndrome. *J Clin Biochem Nutr* 59: 107-112
Jin JO, Shinohara Y, Yu Q (2013) Innate immune signaling induces interleukin-7 production from salivary gland cells and accelerates the development of primary Sjogren's syndrome in a mouse model. *PLoS One* 8: e77605
Jonsson MV, Delaleu N, Brokstad KA, Berggreen E, Skarstein K (2006) Impaired salivary gland function in nod mice - Association with changes in cytokine profile but not with salivary gland histopathology. *Arthritis Rheum-Us* 54: S707-S707
Kim D, Paggi JM, Park C, Bennett C, Salzberg SL (2019) Graph-based genome alignment and genotyping with HISAT2 and HISAT-genotype. *Nat Biotechnol* 37: 907-915
Kim S, Lee K, Choi YS, Ku J, Lee YJ, Kim Y (2020) Mitochondrial dsRNAs activate PKR and TLR3 to promote chondrocyte degeneration in osteoarthritis. *bioRxiv*: 2020.2006.2017.156323
Kim Y, Park J, Kim S, Kim M, Kang MG, Kwak C, Kang M, Kim B, Rhee HW, Kim VN (2018) PKR Senses Nuclear and Mitochondrial Signals by Interacting with Endogenous Double-Stranded RNAs. *Mol Cell* 71: 1051-1063 e1056
Kiripolsky J, Kramer JM (2018) Current and Emerging Evidence for Toll-Like Receptor Activation in Sjogren's Syndrome. *J Immunol Res* 2018: 1246818
Kroese FG, Abdulahad WH, Haacke E, Bos NA, Vissink A, Bootsma H (2014) B-cell hyperactivity in primary Sjogren's syndrome. *Expert Rev Clin Immunol* 10: 483-499
Lagouge M, Mourier A, Lee HJ, Spahr H, Wai T, Kukat C, Silva Ramos E, Motori E, Busch JD, Siira S *et al* (2015) SLIRP Regulates the Rate of Mitochondrial Protein Synthesis and Protects LRPPRC from Degradation. *PLoS Genet* 11: e1005423
Lee BH, Gauna AE, Perez G, Park YJ, Pauley KM, Kawai T, Cha S (2013) Autoantibodies against muscarinic type 3 receptor in Sjogren's syndrome inhibit aquaporin 5 trafficking. *PLoS One* 8: e53113
Lee H, Fenster RJ, Pineda SS, Gibbs WS, Mohammadi S, Davila-Velderrain J, Garcia FJ, Therrien M, Novis HS, Gao F *et al* (2020a) Cell Type-Specific Transcriptomics Reveals that Mutant Huntingtin Leads to Mitochondrial RNA Release and Neuronal Innate Immune Activation. *Neuron* 107: 891-908 e898
Lee J, Lee J, Kwok SK, Baek S, Jang SG, Hong SM, Min JW, Choi SS, Lee J, Cho ML *et al* (2018) JAK-1 Inhibition Suppresses Interferon-Induced BAFF Production in Human Salivary Gland: Potential Therapeutic Strategy for Primary Sjogren's Syndrome. *Arthritis Rheumatol* 70: 2057-2066

Lee JH, Shim YR, Seo W, Kim MH, Choi WM, Kim HH, Kim YE, Yang K, Ryu T, Jeong JM *et al* (2020b) Mitochondrial Double-Stranded RNA in Exosome Promotes Interleukin-17 Production Through Toll-Like Receptor 3 in Alcohol-associated Liver Injury. *Hepatology* 72: 609-625
Lee YJ, Scofield RH, Hyon JY, Yun PY, Lee HJ, Lee EY, Lee EB, Song YW (2010) Salivary chemokine levels in patients with primary Sjogren's syndrome. *Rheumatology (Oxford)* 49: 1747-1752
Li JC, Ha YM, Ku NY, Choi SY, Lee SJ, Oh SB, Kim JS, Lee JH, Lee EB, Song YW *et al* (2004) Inhibitory effects of autoantibodies on the muscarinic receptors in Sjogren's syndrome. *Laboratory Investigation* 84: 1430-1438
Lopez-Lopez J, Jane Salas E, Chimenos Kustner E (2014) [Prognosis and treatment of dry mouth. Systematic review]. *Med Clin (Barc)* 142: 119-124
Lopez-Pintor RM, Fernandez Castro M, Hernandez G (2015) Oral involvement in patients with primary Sjogren's syndrome. Multidisciplinary care by dentists and rheumatologists. *Reumatol Clin* 11: 387-394
Love MI, Huber W, Anders S (2014) Moderated estimation of fold change and dispersion for RNA-seq data with DESeq2. *Genome Biol* 15: 550
Ma Z (2012) Total RNA Extraction from Formalin-Fixed, Paraffin-Embedded (FFPE) Blocks. *Bio-protocol* 2: e161
Maria NI, Steenwijk EC, AS IJ, van Helden-Meeuwsen CG, Vogelsang P, Beumer W, Brkic Z, van Daele PL, van Hagen PM, van der Spek PJ *et al* (2017) Contrasting expression pattern of RNA-sensing receptors TLR7, RIG-I and MDA5 in interferon-positive and interferon-negative patients with primary Sjogren's syndrome. *Ann Rheum Dis* 76: 721-730
McInnes IB, Byers NL, Higgs RE, Lee J, Macias WL, Na S, Ortmann RA, Rocha G, Rooney TP, Wehrman T *et al* (2019) Comparison of baricitinib, upadacitinib, and tofacitinib mediated regulation of cytokine signaling in human leukocyte subpopulations. *Arthritis Res Ther* 21: 183
Min HK, Moon SJ, Park KS, Kim KJ (2019) Integrated systems analysis of salivary gland transcriptomics reveals key molecular networks in Sjogren's syndrome. *Arthritis Res Ther* 21: 294
Minagi HO, Ikai K, Araie T, Sakai M, Sakai T (2018) Benefits of long-term pilocarpine due to increased muscarinic acetylcholine receptor 3 in salivary glands. *Biochem Bioph Res Co* 503: 1098-1102
Miranda-Rius J, Brunet-Llobet L, Lahor-Soler E, Farre M (2015) Salivary Secretory Disorders, Inducing Drugs, and Clinical Management. *Int J Med Sci* 12: 811-824
Mona M, Mondello S, Hyon JY, Saleh W, Han K, Lee HJ, Ha YJ, Kang EH, Lee YJ, Cha S (2020) Clinical usefulness of anti-muscarinic type 3 receptor autoantibodies in patients with primary Sjogren's syndrome. *Clin Exp Rheumatol*
Pagano G, Castello G, Pallardo FV (2013) Sjogren's syndrome-associated oxidative stress and mitochondrial dysfunction: prospects for chemoprevention trials. *Free Radic Res* 47: 71-73
Park YS, Gauna AE, Cha S (2015) Mouse Models of Primary Sjogren's Syndrome. *Curr Pharm Des* 21: 2350-2364
Passafaro D, Reina S, Sterin-Borda L, Borda E (2010) Cholinergic autoantibodies from primary Sjogren's syndrome modulate submandibular gland Na+/K+-ATPase activity via prostaglandin E2 and cyclic AMP. *Eur J Oral Sci* 118: 131-138
Pena-Blanco A, Garcia-Saez AJ (2018) Bax, Bak and beyond - mitochondrial performance in apoptosis. *FEBS J* 285: 416-431

Pertea M, Pertea GM, Antonescu CM, Chang TC, Mendell JT, Salzberg SL (2015) StringTie enables improved reconstruction of a transcriptome from RNA-seq reads. *Nat Biotechnol* 33: 290-295
Qin B, Wang J, Yang Z, Yang M, Ma N, Huang F, Zhong R (2015) Epidemiology of primary Sjogren's syndrome: a systematic review and meta-analysis. *Ann Rheum Dis* 74: 1983-1989
Rai P, Janardhan KS, Meacham J, Madenspacher JH, Lin WC, Karmaus PWF, Martinez J, Li QZ, Yan M, Zeng J *et al* (2021) IRGM1 links mitochondrial quality control to autoimmunity. *Nat Immunol* 22: 312-321
Riley JS, Tait SW (2020) Mitochondrial DNA in inflammation and immunity. *EMBO Rep* 21: e49799
Robinson CP, Brayer J, Yamachika S, Esch TR, Peck AB, Stewart CA, Peen E, Jonsson R, Humphreys-Beher M (1998) Transfer of human serum IgG to nonobese diabetic Ig mu(null) mice reveals a role for autoantibodies in the loss of secretory function of exocrine tissues in Sjogren's syndrome. *Arthritis Rheum-Us* 41: S354-S354
Ryo K, Yamada H, Nakagawa Y, Tai Y, Obara K, Inoue H, Mishima K, Saito I (2006) Possible involvement of oxidative stress in salivary gland of patients with Sjogren's syndrome. *Pathobiology* 73: 252-260
Schenke-Layland K, Xie JS, Angelis E, Starcher B, Wu KJ, Riemann I, MacLellan WR, Hamm-Alvarez SF (2008) Increased degradation of extracellular matrix structures of lacrimal glands implicated in the pathogenesis of Sjogren's syndrome. *Matrix Biology* 27: 53-66
Shiboski CH, Shiboski SC, Seror R, Criswell LA, Labetoulle M, Lietman TM, Rasmussen A, Scofield H, Vitali C, Bowman SJ *et al* (2017) 2016 American College of Rheumatology/European League Against Rheumatism Classification Criteria for Primary Sjogren's Syndrome: A Consensus and Data-Driven Methodology Involving Three International Patient Cohorts. *Arthritis Rheumatol* 69: 35-45
Stefanski AL, Tomiak C, Pleyer U, Dietrich T, Burmester GR, Dorner T (2017) The Diagnosis and Treatment of Sjogren's Syndrome. *Dtsch Arztebl Int* 114: 354-361
Steinfeld S, Cogan E, King LS, Agre P, Kiss R, Delporte C (2001) Abnormal distribution of aquaporin-5 water channel protein in salivary glands from Sjogren's syndrome patients. *Lab Invest* 81: 143-148
Vitali C, Bombardieri S, Jonsson R, Moutsopoulos HM, Alexander EL, Carsons SE, Daniels TE, Fox PC, Fox RI, Kassan SS *et al* (2002) Classification criteria for Sjogren's syndrome: a revised version of the European criteria proposed by the American-European Consensus Group. *Ann Rheum Dis* 61: 554-558
Whitcher JP, Shiboski CH, Shiboski SC, Heidenreich AM, Kitagawa K, Zhang S, Hamann S, Larkin G, McNamara NA, Greenspan JS *et al* (2010) A simplified quantitative method for assessing keratoconjunctivitis sicca from the Sjogren's Syndrome International Registry. *Am J Ophthalmol* 149: 405-415
You H, Xu D, Zhao J, Li J, Wang Q, Tian X, Li M, Zeng X (2020) JAK Inhibitors: Prospects in Connective Tissue Diseases. *Clin Rev Allergy Immunol* 59: 334-351
Yu SJ, Choi G, Cho Y, Lee M, Cho Y, Shin JH, Lee E, Im SG (2020) Three-Dimensional Spheroid Culture on Polymer-Coated Surface Potentiate Stem Cell Functions via Enhanced Cell-Extracellular Matrix Interactions. *Acs Biomater Sci Eng* 6: 2240-2250
Zhang J, Ney PA (2009) Role of BNIP3 and NIX in cell death, autophagy, and mitophagy. *Cell Death Differ* 16: 939-946

Zhang LW, Cong X, Zhang Y, Wei T, Su YC, Serrao AC, Brito AR, Jr., Yu GY, Hua H, Wu LL (2016) Interleukin-17 Impairs Salivary Tight Junction Integrity in Sjogren's Syndrome. *J Dent Res* 95: 784-792
Zhou J, Jin JO, Du J, Yu Q (2015) Innate Immune Signaling Induces IL-7 Production, Early Inflammatory Responses, and Sjogren's-Like Dacryoadenitis in C57BL/6 Mice. *Invest Ophthalmol Vis Sci* 56: 7831-7838

Figure Legends

Fig. 1. mt-dsRNAs are elevated in saliva and tears of SS patients as well as salivary gland tissues of aged NOD mice. (**A**) The experimental scheme. To distinguish between mt-dsRNAs from the heavy and light strands, strand-specific reverse transcription was used to synthesize cDNAs. (**B**) The relative RNA expression levels of both heavy (H) and light (L) strands in saliva among non-sicca control, non-SS sicca and SS patients. (**C**) The relative RNA expression levels in tears between non-SS sicca and SS patients. All Cq values are relative to *GAPDH* mRNA, then normalized to non-sicca and non-SS sicca controls. (**D**) Expression levels of five SS-associated mt-dsRNAs in the salivary gland of NOD mice. All Cq values are relative to *Actb* mRNA, then normalized to 8-week old NOD mouse samples. Results are presented as the mean ± SEM of three independent samples. (**E**) Representative fluorescence images of NOD mouse salivary gland tissues with mt-Nd5 light (*Nd5L*) and heavy strand (*Nd5H*) transcripts. (**F**) The negative control probe yielded no signal. For (**E**) and (**F**), the scale bar represents 50 µm.

Fig. 2. dsRNA stimulation induces autoimmune features of SS and mt-dsRNA expression in SGECs spheroids. (**A**) A schematic representation of 3D culture by depositing V4D4 monomers via iCVD process. (**B**) The relative mRNA expression of indicated ISGs in poly I:C transfected NS-SV-AC spheroids. RNA was isolated and the indicated ISGs expressions were quantified by qRT-PCR. Shown are normalized $\log_2$ fold enrichment of three independent experiments with error bars denoting SEM. All Cq values are relative to *ACTB* mRNA, then normalized to Mock transfected control. (**C**) Western blot analysis of PKR phosphorylation upon poly I:C transfection in 3D system. (**D**) APH assay showing cell viability upon poly I:C transfection. Shown are four independent experiments with error bars denoting SEM. (**E-G**) Poly I:C transfection led to

decreased TJC and AQP5-GFP expressions. (**E**) Representative fluorescence images of ZO-1 and Occludin upon poly I:C transfection. (**F**) Representative fluorescence images of AQP5-GFP upon poly I:C transfection. The fluorescence intensities were quantified as the mean of three independent experiments and normalized to the Mock transfection control group. For (**E**) and (**F**), the scale bar represents 100 µm. (**G**) Western blot analysis of AQP5-GFP expression upon poly I:C transfection. (**H**) The relative mt-dsRNA expression in poly I:C transfected NS-SV-AC spheroids. RNA was isolated and mt-dsRNA expressions were quantified by qRT-PCR. Shown are normalized $\log_2$ fold enrichment of three independent experiments with error bars denoting SEM. All Cq values are relative to *ACTB* mRNA, then normalized to Mock transfected control. All statistical significances were calculated using one-tailed Student's t-tests, $*p \leq 0.05$, $**p \leq 0.01$, and $***p \leq 0.001$.

Fig. 3. mt-dsRNA induction occurs downstream of the JAK1 signaling pathway. NS-SV-AC spheroids were pretreated with upadacitinib 1 h prior to poly I:C stimulation. From the isolated RNAs, the expression levels of eight ISGs (**A**), and mt-dsRNAs (**B**) were quantified by qRT-PCR. All Cq values are relative to *ACTB* mRNA. For upadacitinib-untreated control (CTRL), values of poly I:C-transfected samples were normalized to Mock-transfected samples. The same normalization was carried out for upadacitinib-treated samples. The degree of induction with or without upadacitinib pretreatment was then compared by computing the ratio between CTRL and upadacitinib-treated poly I:C-transfected samples. Shown are three independent experiments with error bars denoting SEM. All statistical significances were calculated using one-tailed Student's t-tests, $*p \leq 0.05$, $**p \leq 0.01$, and $***p \leq 0.001$.

Fig. 4. M3R ligand Ach prevents mt-dsRNA induction to yield the protective effects against SS-like autoimmune phenotypes. NS-SV-AC spheroids were stimulated with poly I:C in the presence or the absence of 100 μM Ach. From the isolated RNAs, the expression levels of eight ISGs (**A**), and mt-dsRNAs (**B**) were quantified by qRT-PCR. All Cq values are relative to *ACTB* mRNA. For the control group, values of poly I:C-transfected samples were normalized to Mock-transfected samples. The same normalization was carried out for samples transfected with poly I:C in the presence of Ach. The degree of induction in the presence or the absence of Ach was then compared by computing the ratio between CTRL and Ach-treated poly I:C-transfected samples. (**C**) NS-SV-AC spheroids were treated with 2-CM, then the expression levels of mt-dsRNAs were measured by qRT-PCR. Shown are six independent experiments with SEM. (**D**) The ratio of ISGs induction upon poly I:C transfection between Ach-treated and control samples in 2-CM-pretreated cells. (**E-F**) NS-SV-AC spheroids were stimulated with poly I:C in the presence of 100 μM Ach and 500 μg of control IgG or SS-IgG. From the isolated RNAs, the expression levels of eight ISGs (**E**), and mt-dsRNAs (**F**) were quantified by qRT-PCR. The degree of induction upon poly I:C transfection in the presence of Ach with or without SS-IgG was compared by computing the ratio between CTRL and SS-IgG-treated poly I:C transfected samples. (**G-H**) The effect of control human IgG was compared with RA-IgG. The degree of ISGs (**G**) and mt-dsRNA (**H**) induction upon poly I:C stimulation in the presence of Ach with either control IgG or RA-IgG was compared by computing the ratio between CTRL and RA-IgG-treated poly I:C transfected samples. (**I**) A schematic representation of intracellular Ach interacting with M3R to prevent mt-dsRNA release to the cytosol. Unless mentioned otherwise, the shown graph represents three independent experiments with error bars denoting SEM. All statistical significances were calculated using one-tailed Student's t-tests, $*p \leq 0.05$, $**p \leq 0.01$, and $***p \leq 0.001$.

Fig. 5. Antioxidant improves SS-like features partly by downregulating mt-dsRNA expression. NS-SV-AC spheroids were pretreated with 20 μM RES 24 h prior to poly I:C stimulation. (**A**) Heatmap of mRNA sequencing results for type I IFN signaling pathway genes. The two columns represent $\log_2$ fold changes with or without RES pretreatment. (**B**) APH assay showing the effect of RES on cell viability. Shown are four independent experiments with error bars denoting SEM. (**C**) Western blot analysis of PKR phosphorylation upon poly I:C stimulation with or without RES pretreatment. (**D**) Representative fluorescence images of ZO-1 and Occludin expression. Similarly, AQP5-GFP expression upon poly I:C stimulation with or without RES pretreatment was analyzed by (**E**) western blot and (**F**) immunocytochemistry. The fluorescence intensities in (**D**) and (**F**) were quantified as the mean of three independent experiments and normalized to the Mock transfection control group. The scale bar represents 100 μm. (**G**) Expression levels of mt-dsRNAs in the poly I:C-stimulated NS-SV-AC with or without RES pretreatment. All Cq values are relative to *ACTB* mRNA. For the control group, values of poly I:C-stimulated samples were normalized to Mock-transfected samples. The same normalization was carried out for RES-pretreated samples. The degree of induction with or without RES pretreatment was then compared by computing the ratio between CTRL and RES-pretreated poly I:C-stimulated samples. Shown are three independent experiments with error bars denoting SEM. All statistical significances were calculated using one-tailed Student's t-tests, $*p \leq 0.05$, $**p \leq 0.01$, and $***p \leq 0.001$.

Fig. 6. Downregulation of mt-dsRNAs reduces the immune response to poly I:C stimulation. **(A)** Heatmap of mRNA sequencing results for type I IFN signaling pathway genes. The two columns represent $\log_2$ fold changes with or without 2-CM pretreatment 24 h prior to poly I:C

stimulation. (**B**) APH assay showing cell viability upon poly I:C stimulation with or without 2-CM pretreatment. Shown are four independent experiments with error bars denoting SEM. (**C**) Western blot analysis of PKR phosphorylation upon poly I:C stimulation with or without 2-CM pretreatment. (**D**) Representative fluorescence images of ZO-1 and Occludin upon poly I:C stimulation with or without 2-CM pretreatment. AQP5-GFP expression upon poly I:C stimulation with or without 2-CM pretreatment was analyzed by (**E**) western blot and (**F**) immunocytochemistry. The fluorescence intensities in (**D**) and (**F**) were quantified as the mean of three independent experiments and normalized to the Mock transfection control group. The scale bar represents 100 μm. All statistical significances were calculated using one-tailed Student's t-tests, *$p \leq 0.05$, **$p \leq 0.01$, and ***$p \leq 0.001$.

Graphical Abstract. mt-dsRNAs as the molecular mediator of autoimmune phenotypes in SS. mt-dsRNAs are elevated in both human samples and mouse model of SS and function to exacerbate dsRNA-induced autoimmune phenotypes in SS. Countering the accumulation of mt-dsRNAs alleviates the autoimmune phenotypes in SGECs.

Figure 1.

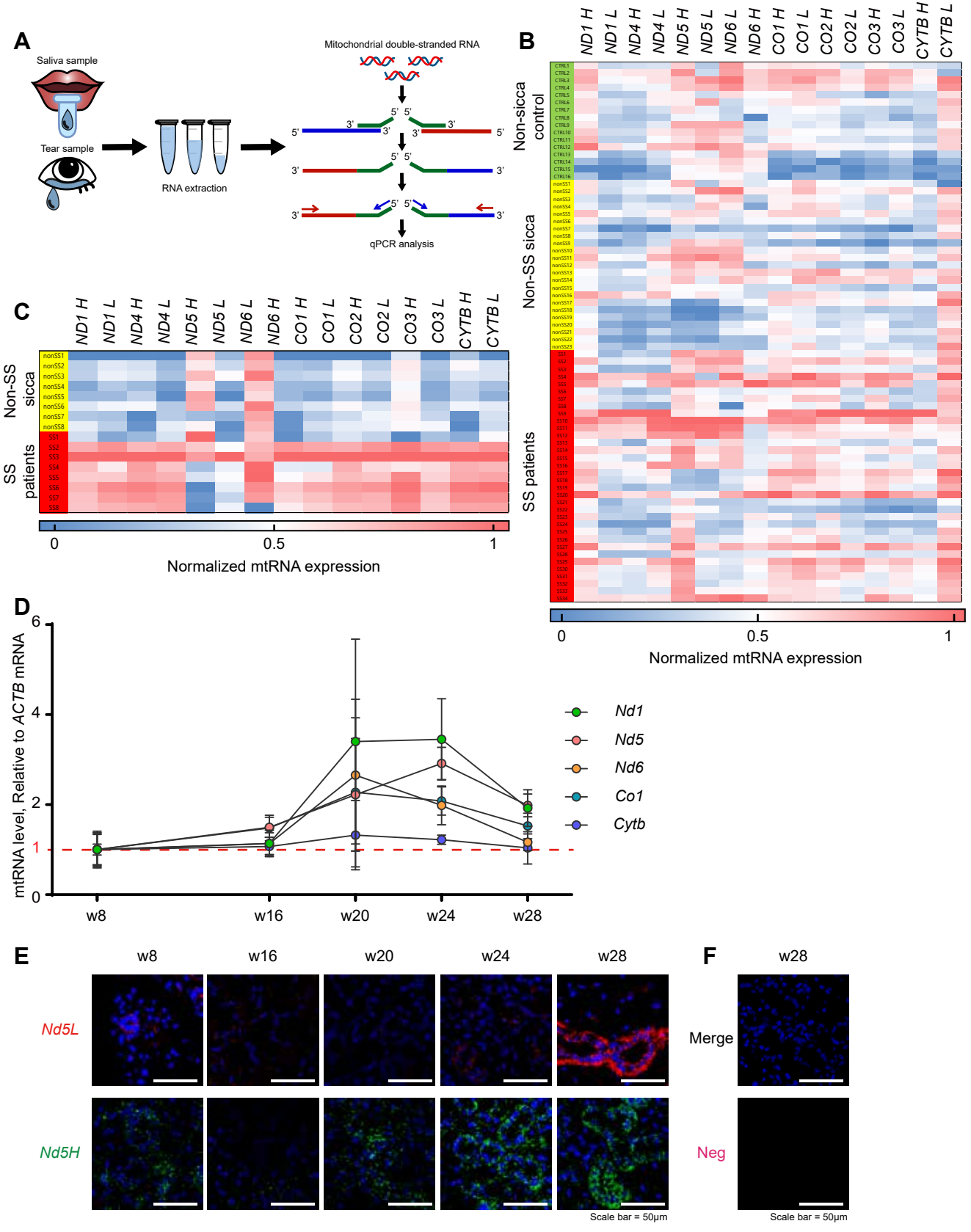
A
Saliva sample
Tear sample
RNA extraction
Mitochondrial double-stranded RNA
qPCR analysis
B
ND1 H
ND1 L
ND4 H
ND4 L
ND5 H
ND5 L
ND6 L
ND6 H
CO1 H
CO1 L
CO2 H
CO2 L
CO3 H
CO3 L
CYTB H
CYTB L
Non-sicca control
Non-SS sicca
SS patients
0
0.5
1
Normalized mtRNA expression
C
Non-SS sicca
SS patients
Normalized mtRNA expression
D
mtRNA level, Relative to ACTB mRNA
w8
w16
w20
w24
w28
Nd1
Nd5
Nd6
Co1
Cytb
E
w8
w16
w20
w24
w28
Nd5L
Nd5H
Scale bar = 50μm
F
w28
Merge
Neg
Scale bar = 50μm

Figure 2.

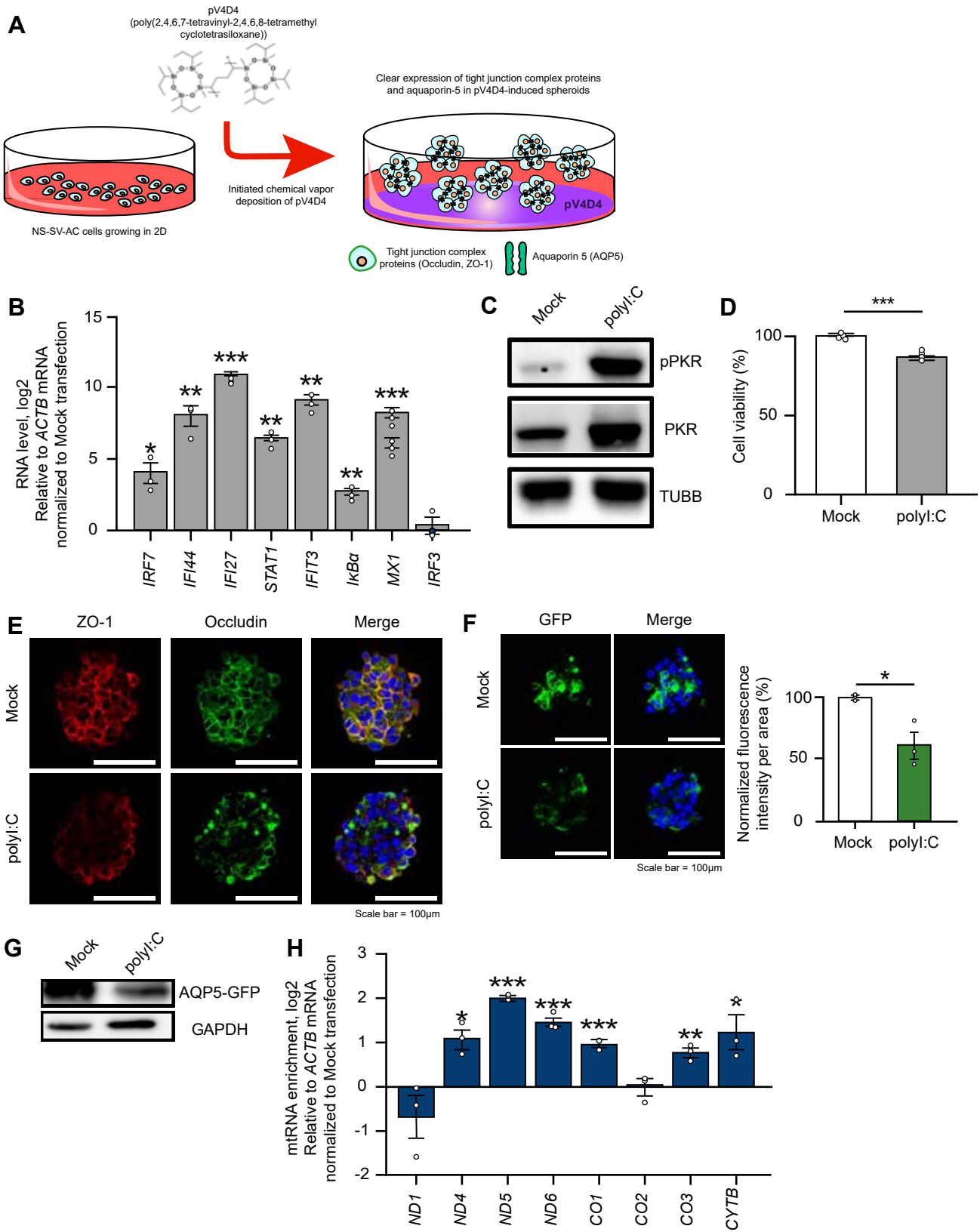
A
pV4D4
(poly(2,4,6,7-tetravinyl-2,4,6,8-tetramethyl cyclotetrasiloxane))
Clear expression of tight junction complex proteins and aquaporin-5 in pV4D4-induced spheroids
Initiated chemical vapor deposition of pV4D4
NS-SV-AC cells growing in 2D
pV4D4
Tight junction complex proteins (Occludin, ZO-1)
Aquaporin 5 (AQP5)
B
RNA level, log2 Relative to ACTB mRNA normalized to Mock transfection
IRF7
IFI44
IFI27
STAT1
IFIT3
IκBα
MX1
IRF3
C
Mock
polyI:C
pPKR
PKR
TUBB
D
Cell viability (%)
Mock
polyI:C
E
ZO-1
Occludin
Merge
Mock
polyI:C
Scale bar = 100μm
F
GFP
Merge
Mock
polyI:C
Scale bar = 100μm
Normalized fluorescence intensity per area (%)
Mock
polyI:C
G
Mock
polyI:C
AQP5-GFP
GAPDH
H
mtRNA enrichment, log2 Relative to ACTB mRNA normalized to Mock transfection
ND1
ND4
ND5
ND6
CO1
CO2
CO3
CYTB

Figure 3.

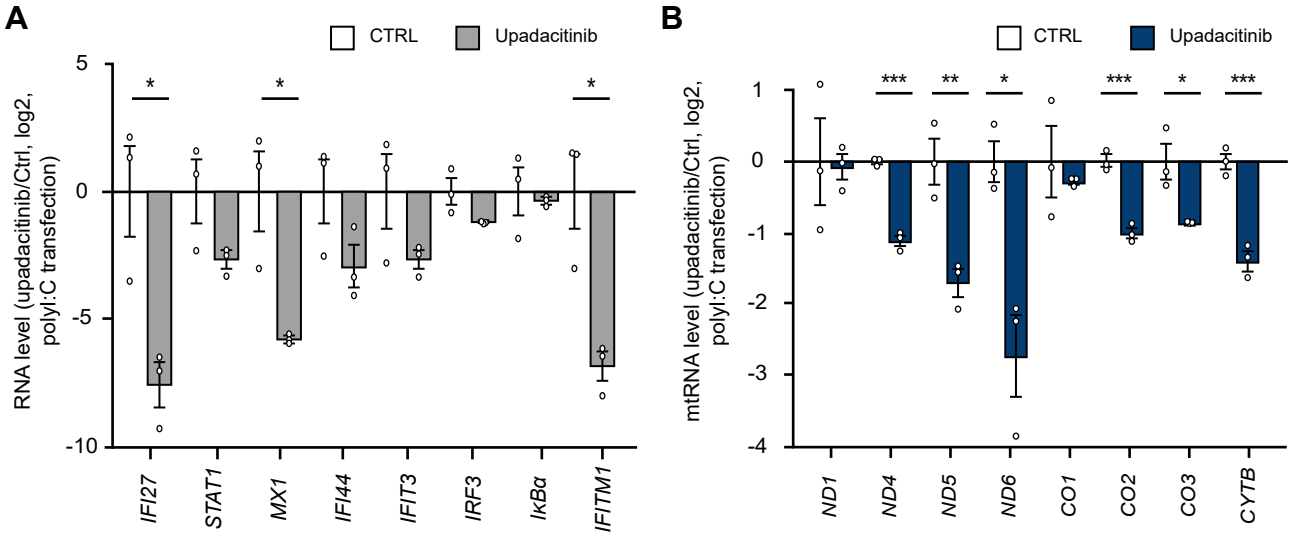
A
CTRL
Upadacitinib
RNA level (upadacitinib/Ctrl, log2, polyI:C transfection)
5
0
-5
-10
*
*
*
IFI27
STAT1
MX1
IFI44
IFIT3
IRF3
IκBα
IFITM1
B
CTRL
Upadacitinib
mtRNA level (upadacitinib/Ctrl, log2, polyI:C transfection)
1
0
-1
-2
-3
-4
***
**
*
***
*
***
ND1
ND4
ND5
ND6
CO1
CO2
CO3
CYTB

Figure 4.

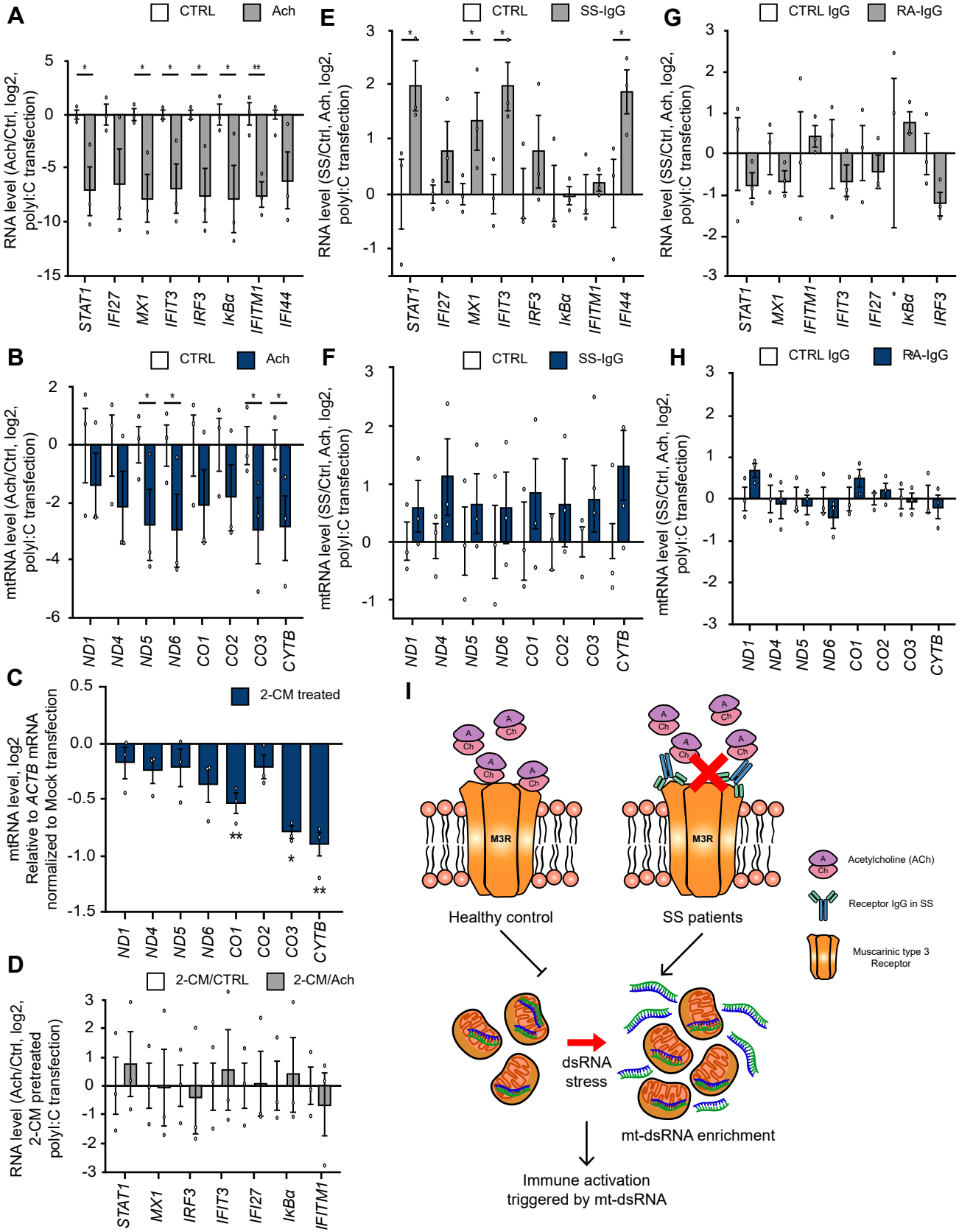
A
CTRL
Ach
RNA level (Ach/Ctrl, log2, polyI:C transfection)
STAT1
IFI27
MX1
IFIT3
IRF3
IκBα
IFITM1
IFI44
B
CTRL
Ach
mtRNA level (Ach/Ctrl, log2, polyI:C transfection)
ND1
ND4
ND5
ND6
CO1
CO2
CO3
CYTB
C
2-CM treated
mtRNA level, log2 Relative to ACTB mRNA normalized to Mock transfection
D
2-CM/CTRL
2-CM/Ach
RNA level (Ach/Ctrl, log2, 2-CM pretreated polyI:C transfection)
E
CTRL
SS-IgG
RNA level (SS/Ctrl, Ach, log2, polyI:C transfection)
F
CTRL
SS-IgG
mtRNA level (SS/Ctrl, Ach, log2, polyI:C transfection)
G
CTRL IgG
RA-IgG
H
CTRL IgG
RA-IgG
I
M3R
Healthy control
SS patients
Acetylcholine (ACh)
Receptor IgG in SS
Muscarinic type 3 Receptor
dsRNA stress
mt-dsRNA enrichment
Immune activation triggered by mt-dsRNA

Figure 5.

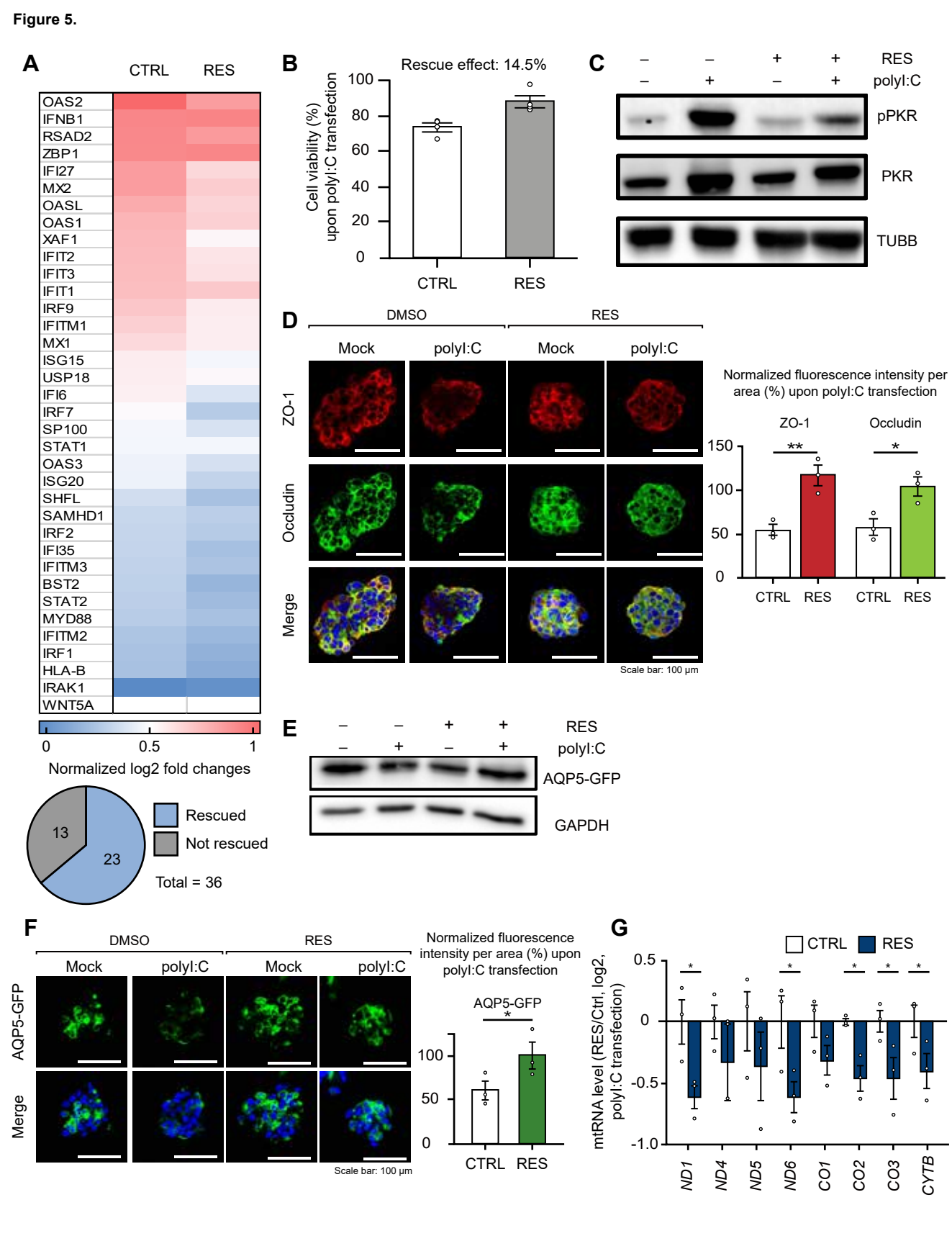
A
CTRL
RES
OAS2
IFNB1
RSAD2
ZBP1
IFI27
MX2
OASL
OAS1
XAF1
IFIT2
IFIT3
IFIT1
IRF9
IFITM1
MX1
ISG15
USP18
IFI6
IRF7
SP100
STAT1
OAS3
ISG20
SHFL
SAMHD1
IRF2
IFI35
IFITM3
BST2
STAT2
MYD88
IFITM2
IRF1
HLA-B
IRAK1
WNT5A
0
0.5
1
Normalized log2 fold changes
13
23
Rescued
Not rescued
Total = 36
B
Rescue effect: 14.5%
Cell viability (%) upon polyI:C transfection
100
80
60
40
20
0
CTRL
RES
C
RES
polyI:C
pPKR
PKR
TUBB
D
DMSO
RES
Mock
polyI:C
Mock
polyI:C
ZO-1
Occludin
Merge
Scale bar: 100 µm
Normalized fluorescence intensity per area (%) upon polyI:C transfection
ZO-1
Occludin
150
100
50
0
**
*
CTRL
RES
CTRL
RES
E
RES
polyI:C
AQP5-GFP
GAPDH
F
DMSO
RES
Mock
polyI:C
Mock
polyI:C
AQP5-GFP
Merge
Scale bar: 100 µm
Normalized fluorescence intensity per area (%) upon polyI:C transfection
AQP5-GFP
*
100
50
0
CTRL
RES
G
CTRL
RES
mtRNA level (RES/Ctrl, log2, polyI:C transfection)
0.5
0
-0.5
-1.0
ND1
ND4
ND5
ND6
CO1
CO2
CO3
CYTB

Figure 6.

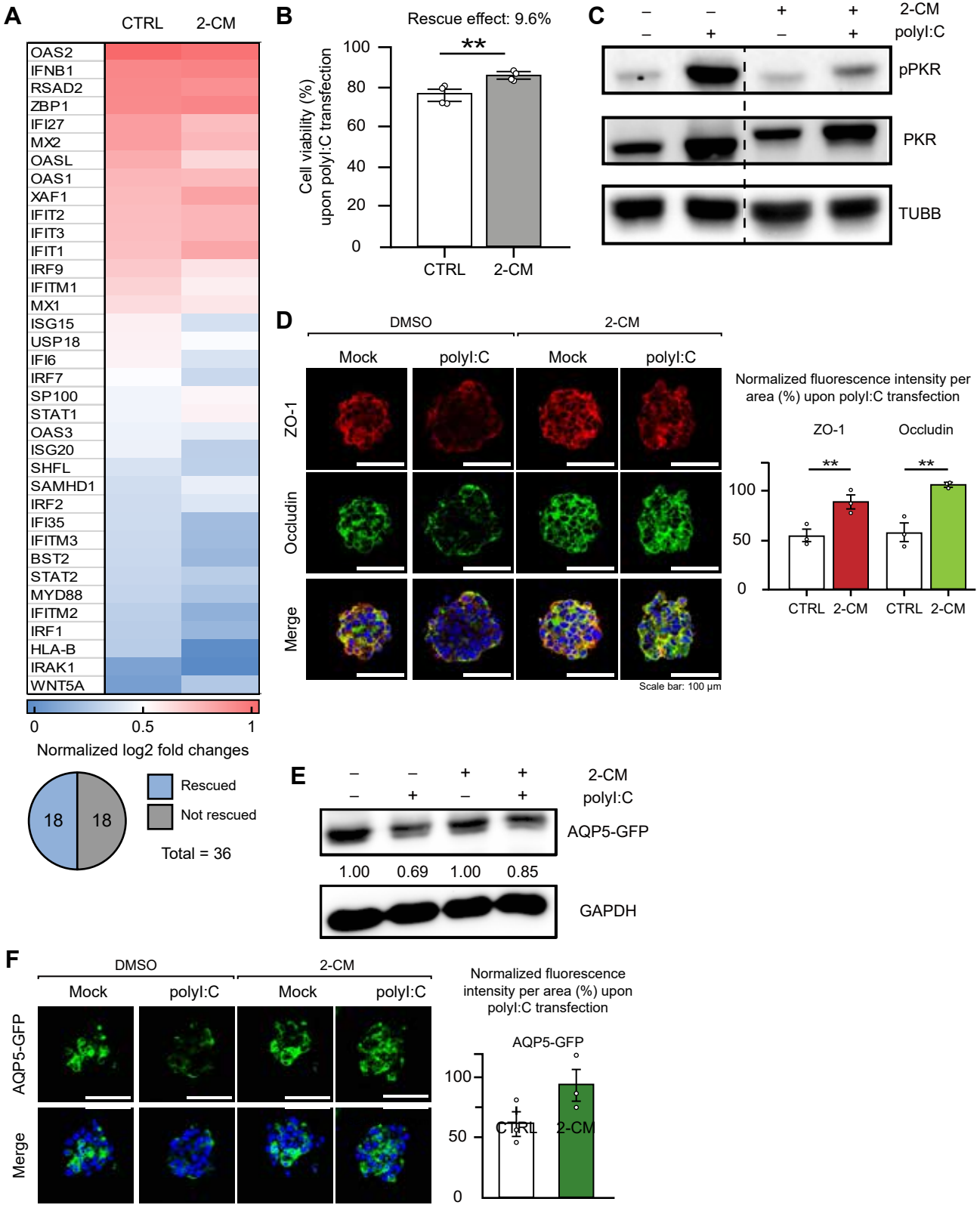
A
CTRL
2-CM
OAS2
IFNB1
RSAD2
ZBP1
IFI27
MX2
OASL
OAS1
XAF1
IFIT2
IFIT3
IFIT1
IRF9
IFITM1
MX1
ISG15
USP18
IFI6
IRF7
SP100
STAT1
OAS3
ISG20
SHFL
SAMHD1
IRF2
IFI35
IFITM3
BST2
STAT2
MYD88
IFITM2
IRF1
HLA-B
IRAK1
WNT5A
0
0.5
1
Normalized log2 fold changes
18
18
Rescued
Not rescued
Total = 36
B
Rescue effect: 9.6%
**
Cell viability (%) upon polyI:C transfection
100
80
60
40
20
0
CTRL
2-CM
C
2-CM
polyI:C
pPKR
PKR
TUBB
D
DMSO
2-CM
Mock
polyI:C
Mock
polyI:C
ZO-1
Occludin
Merge
Scale bar: 100 μm
Normalized fluorescence intensity per area (%) upon polyI:C transfection
ZO-1
Occludin
**
**
100
50
0
CTRL
2-CM
CTRL
2-CM
E
2-CM
polyI:C
AQP5-GFP
1.00
0.69
1.00
0.85
GAPDH
F
DMSO
2-CM
Mock
polyI:C
Mock
polyI:C
AQP5-GFP
Merge
Normalized fluorescence intensity per area (%) upon polyI:C transfection
AQP5-GFP
100
50
0
CTRL
2-CM
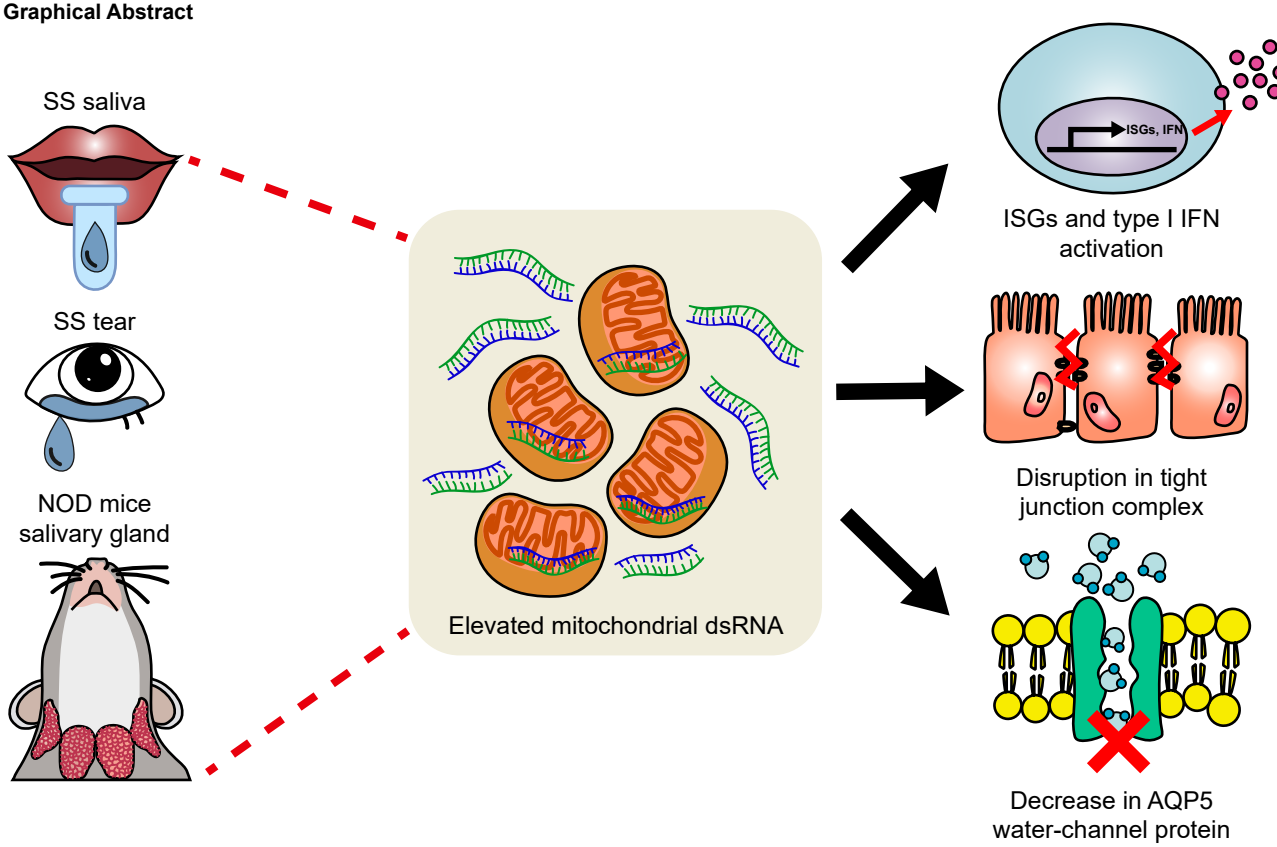
Graphical Abstract